Effects of autogenous healing on the recovery of mechanical performance of High Performance Fibre Reinforced Cementitious Composites (HPFRCCs): part 1

Liberato Ferrara[1,2], Visar Krelani,[1,4], Fabio Moretti[1], Marta Roig Flores[3] and Pedro Serna Ros[3]

ABSTRACT

This paper presents the results are shown of a thorough characterization of the self-healing capacity of High Performance Fibre Reinforced Cementitious Composites (HPFRCCs). The capacity of the material will be investigated to completely or partially re-seal the cracks, as a function of its composition, maximum crack width and exposure conditions. The analysis will also consider different flow-induced alignments of fibres, which can result into either strain-hardening or softening behaviour, whether the material is stressed parallel or perpendicularly to the fibres, respectively. Beam specimens, initially pre-cracked in 4-point bending up to different values of crack opening, were submitted to different exposure conditions, including water immersion, exposure to humid or dry air, and wet-and-dry cycles. After scheduled exposure times, ranging from one month to two years, specimens were tested up to failure according to the same test set-up employed for pre-cracking. Outcomes of the self-healing phenomenon, if any, were analyzed in terms of recovery of stiffness, strength and ductility. In a durability-based design framework, self-healing indices quantifying the recovery of mechanical properties were also defined and their significance cross-checked.

[1] Department of Civil and Environmental Engineering, Politecnico di Milano, piazza Leonardo da Vinci 32, 20133 Milano, Italy.
[2] Corresponding author, email: liberato.ferrara@polimi.it
[3] ICITECH – Institute of Concrete Science and Technology, Universitat Politècnica de València, 4N Building Camino de Vera s/n 46022 Valencia, Spain.
[4] now at University for Business and Technology, Kalabria, Prishtinë 10000, Kosova.

1. Introduction

The not seldom dramatic deterioration of existing building structures and infrastructures have revamped in the last decade the technical interest and related research efforts on the self-healing capacity of cement-based construction materials [1,2].

As reportedly known since 1836 (French Academy of Sciences) and as also demonstrated by several tailored or "serendipity" studies all along the last century, even ordinary concrete inherently possesses an "autogenous" self-healing capacity due to either delayed hydration of cement/binder or carbonation, or the combination of both [1,2]. As a matter of fact, because such a capacity turned out to be quite randomly scattered and thus neither reliable nor predictable in an engineering application perspective, a paramount effort is currently challenging the concrete research community: "engineering" self-healing capacity of concrete and cement based construction materials. With that purpose, tailored mix design concepts and related additions are being investigated with the aim of making healing less scattered and hence more reliable, predictable and able to be controlled and regulated as required by the anticipated service and exposure conditions [1-4].

As well known, a discontinuous and randomly dispersed fibre reinforcement in a cement-based matrix is able to effectively control the opening of the cracks and hence provide a reliable support to any kind of self-healing mechanism, in the sense that narrower cracks can be more easily and better healed [5]. In more recent years, a "signature" category of fibre-reinforced cement-based materials has been developed and is going to be increasingly employed, broadly known as High Performance Fibre Reinforced Cementitious Composites (HPFRCCs). The fundamental idea underlying the concept of HPFRCCs is that, once a crack is formed in the matrix and the through-crack fibres start working, the energy required to pull out the fibres at the cracked section

must be higher than the energy required to form a crack at a new position. The iteration of this concept and stress redistribution mechanism up to the complete saturation of the crack spacing, results, before the localization into a single unstably propagating crack, in a stable multi-cracking process in which the opening of each single crack is very effectively controlled and restrained thanks to the bridging effect provided by the fibres. The aforementioned stable multi-cracking process may be associated to a strain-hardening behaviour in direct tension, as well as to a deflection-hardening behaviour in bending, which is likely to bring substantial innovation into concept and design of engineering structures [6].

The composition of HPFRCCs which can yield the mechanical behaviour explained above, is characterized by low maximum aggregate size, high cement and binder content for high compactness of the matrix, low water/binder (w/b) ratio and a fibre volume fraction higher than 1%. Because of the high binder content and low w/b ratio, it is likely that, even after aging, a significant amount of the binder phase remains un-hydrated. Once the cracks form, the un-hydrated binder materials, which generally remain as such in the inner part of a structural element or building component, may come in contact with water, even simply in the form of air moisture, and undergo delayed hydration reactions. The products of these reactions, precipitating onto the crack surfaces, can be able to seal the crack and even heal the material, i.e. provide some recovery of the pristine level of performance in terms of engineering and mechanical properties (i.e. permeability, strength and stiffness, etc.). Moreover, water does not only promote further hydration of cement and binder grains but may also encourage the dissolution and leaching of calcium hydroxide from the cementitious matrix to form calcium carbonate self-healing crystals with the carbon dioxide dissolved in water [7]. Different supplementary cementitious materials, such as fly ash (class C or

F) and slag, also play different role in enhancing the self-healing capacity [8], thanks to their delayed reaction, guaranteeing the repeatability and persistence of the same capacity upon repeated cracking-healing cycles [9].

A few investigations were performed in the past on the self-healing capacity of ordinary Fibre Reinforced Concrete (FRC), with different types of fibres and under different exposure conditions, demonstrating the ability of the tested specimens to recover their strength and stiffness, at different levels depending on the aforementioned variables [1,3,10-12]. Interestingly, it was also observed that in the case of higher volume percentages of fibres, the same fibres were able to better promote self-healing in the sense that they constitute a network supporting the formation and increase of crystals between the faces of the cracks.

Yang et al. [13], investigated the self healing capacity of Engineered Cementitious Composites (ECCs, which can be regarded as a category of HPFRCCs) subjected to different wet and dry conditioning regimes. They found that if the crack width is kept below 150 μm, and even better if below 50 μm, an even complete recovery of the mechanical performance, in terms of strength and ductility can be obtained. Moreover, higher temperatures in the drying stages of the cycles worsened the healing capacity. Li and Li [14] and Yang et al. [15] also found that even in aggressive conditions, such as high-chloride atmosphere or water, the autogenous healing capacity of ECCs is maintained, at level obviously depending on the crack width and aggressiveness of the environment. Snoeck et al. [16] and Snoeck and de Belie [17] also quite recently studied combined synergistic effects of fibres and Super Absorbent Polymers (SAPs) in ECCs whereas Ferrara [18] combined fibres and crystalline admixtures to enhance the self-healing performance of HPFRCCs.

In most recent years, a few studies [19-22] have also been published on the effect that

natural fibres, either alone or in combination with other types of fibre reinforcement, may have on the self-healing capacity of HPFRCCs, mainly in the case of exposure to wet and dry cycles. As a matter of fact, it was found that, due to their porous structure, natural fibres can absorb water during the wetting stages of the cycles and then release it and diffuse throughout the matrix during the drying stages, thus promoting the healing processes more effectively.

In this study, a thorough investigation of the autogenous healing capacity of a typical HPFRCC mix [23], containing 100 kg/m^3 (1.28% by volume) of short straight steel fibres has been performed, considering different exposure conditions. As a distinctive feature of this study, the influence has been investigated of the flow-induced alignment of the fibres on the material behaviour, either deflection-hardening or softening, and on the related self-healing capacity of the cementitious composite. The recovery of load bearing capacity, ductility and stiffness has been evaluated by means of four-point bending tests performed on specimens in the pre-cracked and post-conditioning stages. Suitable healing indicators for the recovery of the aforementioned properties have been defined and quantified in this study through a tailored methodology. In a companion paper [24], the healing recovery indices will be correlated to an Index of Crack Healing, evaluated both through visual image analysis of the healed cracks as well as through a tailored indirect method, proposed by the first authors in a previous study [3]. This method is based on the comparative analysis of the damage evolution curves built for both the pre-cracked and the healed stages from the evaluation of the flexural stiffness. In the authors' opinion, this step represents a fundamental contribution in order to reliably and consistently incorporate the effects of self-healing into tailored durability-based design approaches, based, e.g., on a "healable" crack width threshold concept.

2. Experimental programme

The composition of the HPFRCC employed in the present investigation is shown in Table 1. Slabs 30 mm thick, 1m long and 0.5 m wide were casted. Fibre-reinforced material was poured directly from the mixer onto a chute along one short edge of the moulds, and allowing it to flow parallel to the long sides (Figure 1). From the slabs, once hardened, beam specimens 100 mm wide and 500 mm long were cut to be tested in 4-point bending, according to the schematic also shown in Figure 1. The beam specimens were cut from the slabs so that their axis, and hence the direction of the principal tensile stresses due to the bending action to be applied during the tests, was either parallel or perpendicular to the flow direction of the fresh concrete, along which the fibres are aligned [23, 25-29].

After two or eleven months aging in lab environment, beam specimens were tested in 4-point bending, according to the set-up shown in Figure 2. Tests were performed controlling the actuator displacement, which was applied at a rate equal to 5 μm/sec, and measuring the Crack Opening Displacement (COD) at the beam intrados over a gauge length equal to 200 mm. The test set-up complies with Model Code 2010 guidelines on the design of SFRC structures, where material characterization through tests on un-notched beams is recommended in the case of either structural elements in bending less than 150 mm deep or strain/deflection-hardening FRC, which both apply to the present study. Results of typical tests on specimens bent parallel or perpendicular to the preferential fibre alignment are shown in Figure 3, in terms of nominal bending stress vs. COD curves: the material evidently features a deflection-hardening or softening behaviour whether stressed parallel or orthogonal to the aforementioned flow induced alignment of the fibres. The deflection-hardening behaviour was the result of a stable multi-cracking process in the central part of the specimen (Figure 4a), made

possible by the favourable alignment of the fibres with respect to the applied stress; on the other hand, an unfavourable alignment of the fibres resulted in a single unstably propagating crack (Figure 4b). In view of the aforementioned behaviour, it was decided to pre-crack specimens featuring a deflection softening response (i.e. with fibres perpendicular to the beam axis) up to a COD value equal to 0.5 mm. On the other hand for specimens with fibres parallel to the axis, most likely featuring a deflection-hardening response, three different levels of crack opening were selected and induced in the specimens. Two values of the pre-crack opening were chosen in the pre-peak regime, respectively equal to 1 mm and 2 mm, and one in the post-peak regime equal to (COD_{peak} + 0.5 mm), where COD_{peak} denotes the value of the COD measured in correspondence of the peak stress. It is worth remarking that, because of the stable pre-peak multi-cracking process and of the employed test set-up, the measured value of the COD in the pre-peak regime actually represents the sum of the opening of all the cracks. On the other hand, the value of pre-cracking COD in the post-peak regime has been selected on the basis of an equivalent opening of the unstable localized crack, in analogy to the deflection softening/single cracking case [23, 27].

After pre-cracking, specimens were submitted to different exposure conditions, including: immersion in water at 20°C; exposure to open air in the lab courtyard (temperature and humidity were daily monitored – recorded trends all along the exposure time are shown in Figure 5); exposure in a chamber at constant temperature T = 20°C and relative humidity RH = 95%; exposure in a chamber at constant temperature T = 20°C and relative humidity RH = 50%; wet and dry cycles, consisting of one day in water and one day in the 50% RH chamber.

Different exposure durations were scheduled, namely 1, 6 and 24 months for specimens pre-cracked at the age of 2 months, and 1, 3 and 6 months for specimens pre-cracked

after 11 months aging. The effects of age of pre-cracking (two or eleven months) was considered only for specimens immersed in water, whereas for other exposure conditions only specimens pre-cracked two months after casting were tested. In this way, not only cement hydration but also a significant part of delayed cementitious reaction of slag was completed. This is due to the low water content in the mix, and the need of water/atmosphere moisture to activate the delayed hydration reactions responsible of self-healing. Later age of concrete (11 months) was considered in order to simulate any crack occurring at an indeterminate time during the service life of the structure, complying with reasonable time to accomplish the experimental programme.

For each exposure conditions, reference un-cracked specimens, at the same age of pre-cracking, were also monotonically tested up to failure. A synopsis of the experimental program is given in Table 2.

After the scheduled exposure times, specimens were removed from the conditioning environment, wiped, in case, and, after drying them in lab environment for a few hours, tested up to failure according to the same set-up shown in Figure 2. Superposition between pre-cracking and post-conditioning σ_N-COD curves allowed the evaluation of self-healing capacity and its effects on mechanical performance of the material, as a function of the testing variables listed above.

Ultrasonic Pulse Velocity (UPV) tests were also performed according to the set-up shown in Figure 6 at three steps: 1) before pre-cracking, 2) after pre-cracking but before starting the conditioning and 3) after conditioning but before the final failure tests. Variations in the wave speed associated with crack healing were thus evaluated. Since the wave speed in a solid medium is related to its stiffness, UPV tests provided a complementary (indirect) measure to be jointly analysed with the data garnered through mechanical tests to evaluate the recovery of stiffness. Cross comparison will be thus

instrumental at assessing the reliability of the same data as well as of the tailored analysis procedure, through which "healing indices" for different analysed mechanical properties will be defined and calculated. It is worth remarking that, besides the measurements taken in the central region of the specimen (1-2 in Figure 6), which allowed to evaluate the effects of crack sealing/healing, measurements in the edge portion of the same specimen (0-1 in Figure 6) were also garnered and used to evaluate the effect due to the delayed bulk hydration. Both measurements allowed to discriminate whether the detected recovery of mechanical properties was strictly due to self-healing and/or also to delayed bulk hydration.

3. Experimental results

The results of the pre-cracking and post-conditioning 4-point bending tests, performed as described in the previous section, have been plotted in terms of nominal bending stress σ_N vs. COD curves, for the different investigated pre-crack openings and exposure conditions. Distinction has been made between deflection-softening (Figure 7) and deflection-hardening specimens (Figures 8-10) as well as considering the different pre-cracking ages (2 months – Figure 7 to 10; 11 months Figure 11).

In order to better enable the comprehension of the healing effects on the recovery of the mechanical performance, primarily in terms of load-bearing and deformation capacity, all the curves, including those of reference un-cracked specimens, have been plotted in dimensionless form. Reference has been made either to the peak strength and crack opening, for deflection softening specimens and deflection hardening ones pre-cracked after the peak, or to the pre-cracking stress and crack opening, for deflection hardening specimens pre-cracked in the pre-peak regime.

By comparing for each and all the specimens, the curves in the pre-cracking regime

with that in the post-conditioning one, or with the response of the reference un-cracked specimens, suitable indices will be defined to quantify the effects of healing on the recovery of the load bearing capacity, ductility, flexural stiffness and toughness, as hereafter detailed.

3.1 Index of Strength Recovery

3.1.1 Deflection-softening specimens

In the case of deflection-softening specimens, the effectiveness of healing in promoting the recovery of the "through crack" residual stress bearing capacity can be evaluated by calculating the amount of strength gained after the conditioning period, with respect to the residual strength featured at the maximum pre-crack opening, and comparing it to the stress loss exhibited by the same specimen when pre-cracked up to the aforementioned crack opening threshold (Figure 12). With reference to the notation in the same Figure, the Index of Strength Recovery (ISR) is defined as follows:

$$\text{Index of Strength Recovery ISR} = \frac{f_{peak,\,post\,conditioning} - \sigma_{N\,unloading,pre\text{-}cracking}}{f_{peak,\,pre-cracking} - \sigma_{N\,unloading,pre\text{-}cracking}} \quad (1)$$

From the plots shown in Figures 13a-b it holds that:

- specimens immersed in water, together with specimens exposed to 90% RH, featured, in average, the highest, and a quite similar, recovery trend, able to gain, in the post-conditioning stage and after quite longer exposure times, a strength even slightly higher that the cracking strength of the virgin specimen;
- specimens pre-cracked at 11 months and immersed in water, featured a moderate and moderately increased healing capacity with prolonged immersion;
- specimens exposed to air featured an initial appreciable healing rate, but without any further significant improvement with prolonged exposure time. Besides the

discontinuous availability of water, this can be also reliably attributed to the fact that the (quite high) humidity of the environment initially triggered delayed hydration reactions, which started sealing the crack from its mouth and to such an extent to prevent further effective penetration of the water molecules, also more difficultly available because dispersed in air. Moreover, carbonation reactions, if any, only involved the $Ca(OH)_2$ available on the crack surfaces, no leaching from the inner matrix being possible in such a condition.

It is worth remarking that, for immersed specimens, water could penetrate deeper into the cracks and promote to a larger extent and for longer time delayed hydration reactions, originating from the tip of the crack. Moreover, being the specimens completely immersed, leaching of $Ca(OH)_2$ would also be possible, promoting more effective carbonation reactions with the CO_2 dissolved in the water, fully and continuously available. The precipitation of $CaCO_3$ crystals would be, in an initial stage, slower than leaching, thus allowing further water to penetrate and making it possible for delayed hydration reactions to proceed for longer exposure times.

- as expected, specimens exposed to a dry environment featured an almost negligible healing, even if somewhat increasing with prolonged exposure time, thus compensative the worsening effects of the drying;
- performance under wet and dry cycles was initially relatively poor, even if a strong increase after six months, with no further improvement, was measured.

3.1.2 Deflection-hardening specimens

In the case of deflection-hardening specimens pre-cracked in the pre-peak regime, i.e. at a COD value equal to either 1 mm or 2 mm, the amount of stress bearing capacity recovered due to healing has to be carefully evaluated. As a matter of fact, since the pre-

cracking threshold was set before the specimen could attain its peak and enter into the stage of unstable propagation of the localized crack (softening), a deflection-hardening (wrongly interpretable as strength gain) would have anyway occurred even in instantaneous unloading-reloading tests. The strength gain measured after the conditioning has hence to be suitably cleansed of the aforementioned deflection-hardening capacity that the specimens do inherently possess.

In this framework, with reference to the notation explained in Figure 14a, the Index of Strength Recovery for deflection-hardening specimens pre-cracked in the pre-peak regime is defined as follows:

Index of Strength Recovery ISR =

$$\frac{\left(f_{peak,post-conditioning} - \sigma_{\text{N, unloading pre-crack}}\right) - \dfrac{f_{peak,virgin} - \sigma_{\text{N, unloading, virgin}}}{\sigma_{\text{N, unloading,virgin}}}\sigma_{\text{N, unloading pre-crack}}}{\left(f_{peak,virgin} - \sigma_{\text{N, unloading, virgin}}\right)\dfrac{\sigma_{\text{N,unloading, pre-crack}}}{\sigma_{\text{N, unloading virgin}}}} = \frac{\left(f_{peak,post-conditioning} - \sigma_{\text{N unloainhg pre-crack}}\right)}{\left(f_{peak,virgin} - \sigma_{\text{N, unloading, virgin}}\right)}\frac{\sigma_{\text{N,unloading, virgin}}}{\sigma_{\text{N, unloading pre-crack}}} - 1 \qquad (2)$$

where the term $\dfrac{f_{peak,virgin} - \sigma_{\text{N, unloading, virgin}}}{\sigma_{\text{N, unloading,virgin}}}\sigma_{\text{N, unloading pre-crack}}$ rightly represents the amount of load bearing capacity that the specimen, due to its deflection-hardening behaviour, would have anyway gained after the pre-cracking test.

In the case of deflection-hardening specimens pre-cracked up to 0.5 mm after the attainment of the peak stress, the ISR is calculated as in Equation (1) for deflection softening specimens (Figure 14b) since, similarly to what happened for deflection softening specimens, the pre-cracking brought already the specimen into the stage of the unstable localized crack propagation. It is worth remarking that in the case of deflection-softening specimens, in which only one crack formed, the ISR does really represent what is due to the healing of that same single crack. On the other hand, in the

case of deflection-hardening specimens pre-cracked after the peak, the value of the ISR computed as above will incorporate the effects of healing both the single localized cracks and also all the other multiple cracks which have been formed up to the peak.

The trends of ISR for deflection-hardening specimens for the different pre-crack opening cases herein investigated, are shown in Figures 15 a-c (respectively for pre-cracking up to 1 mm, 2 mm and 0.5 mm after the peak stress). With very few exceptions, which can reasonably be attributed to some random experimental scattering, the trends and influence of exposure conditions are likely to be confirmed, as discussed in detail for deflection-softening specimens. Furthermore it can be observed, as already with reference to deflection-softening specimens, that the on-going healing of cracks was also instrumental to overcome the damage that, in some cases (see e.g. specimens pre-cracked up to 0.5 mm after the peak) was caused by some non-favourable exposure conditions (dry environment, or even for older specimens immersion in water).

Significantly, in the case of specimens pre-cracked after the peak and before the peak at 2 mm crack opening, for the most favourable exposure conditions (such as water immersion or even wet and dry cycles), the recovery did not significantly proceed upon exposures longer than 6 months. As a matter of fact, the already almost completely sealed cracks may have reliably prevented any further ingress of the activator of the reaction (water) and the quite impervious matrix also prevented any further hydration of the bulk matrix. Moreover, for specimens pre-cracked at 11 months age, the recovery of the load bearing capacity was in some cases initially less significant, whereas it proceeded much faster henceforth, reasonably due to a slower activation of the delayed hydration of older un-hydrated binder particles.

The faster and, evidently, better strength recovery exhibited by specimens pre-cracked at 2 mm, than those at 1 mm, may lead us to draw some preliminary conclusions about

the effects of crack opening on the whole healing process. As a matter of fact, because of the multi-cracking, each single crack is likely to be opened, in average, between 150 and 200 μm, and about half of that, for specimens pre-cracked at 2mm and 1mm respectively. In such a crack-opening range, as also confirmed by a previous study on NSC [3], a compromise between the opening of the crack and its "healability" has to be achieved: a wider – in the range detailed above, and deeper penetrating, crack may promote better healing, in a twofold sense. On the one hand, it facilitates the ingress of water and, on the other, it exposes to the action of this a larger amount of un-hydrated binder particle clusters.

3.2 Index of ductility recovery

As it can be observed from typical stress crack-opening pre-crack and post-conditioning curves for deflection-hardening specimens (Figures 8-10 and 14), the self-healing reactions, besides a recovery of the load bearing capacity, assessed and evaluated as in the previous subsection, are likely to affect the deformation capacity, i.e. the ductility of the specimens. This can be clearly seen, in the case of specimens pre-cracked in the pre-peak stage, from the values of the Crack Opening Displacement measured at the peak load in the post-conditioning stage tests, which are higher than the ones measured for the un-cracked virgin specimens, even after same curing time and conditions as the ones underwent by the pre-cracked specimens.

Coherently with the engineering concept of ductility, an Index of Ductility Recovery, IDuR, has been defined as follows, for specimens pre-cracked in the pre-peak stage (Figure 16a):

$$\text{Index of Ductility Recovery IDuR} = \frac{\left(COD_{peak,post-conditioning} - COD_{1st\ crack,\ pre-crack}\right)}{\left(COD_{peak,virgin} - COD_{1stcrack,virgin}\right)} - 1 \quad (3)$$

As a matter of fact, this index compares the gain in ductility that the specimens exhibits

because of self-healing to the ductility that the virgin specimen would have anyway inherently exhibited.

For specimens pre-cracked beyond the peak, IDuR is simply defined as (Figure 16b):

$$\text{Index of Ductility Recovery IDuR} = \frac{\left(COD_{peak,\,post-conditioning} - COD_{unloading,\,pre-crack}\right)}{\left(COD_{peak,\,pre-crack} - COD_{1stcrack,\,pre-crack}\right)} \quad (4)$$

It can be observed (Figures 17 a-c) that all specimens feature a recovery of the ductility, even if with a decreasing trend upon prolonged exposure and that only for some selected crack openings and exposure conditions the ductility of the healed specimens remains higher than that of the reference virgin one. Moreover, specimens pre-cracked beyond the peak provided quite scattered results for which any trend was hardly detectable, even if the worsening with respect to the virgin specimens performance was always confirmed. Interestingly, as far as the effect of the exposure conditions is concerned, it looks that the exposure to open air provides a better recovery of the ductility than immersion in water, which, on its hand, was deemed to be the most favourable conditions to healing with reference to the recovery of load bearing capacity. Finally, wet and dry cycles promote an initial quite significant gain of ductility, up to six months exposure, followed by a rather dramatic loss.

This trend can be reasonably attributed to the fact that healing products closing the crack and restoring the cross-crack continuity of the material, on the one hand restored the load bearing capacity of the material itself. On the other hand, this effect was confined to the same crack location and had scant if not detrimental effect on the stress redistribution capacity upon the re-opening of the same crack when reloading the specimen after conditioning exposure.

In order to have a deeper insight into the effects of self-healing on the flexural ductility of the material, a different calculation procedure, rather related to the post-peak stage is hereafter proposed (Figure 18a) for specimens pre-cracked before the peak:

$$IDuR_{post\text{-}peak} = \frac{\left(COD_{85\%\,peak,\,post-conditioning} - COD_{peak,\,post-conditioning}\right)}{\left(COD_{85\%\,peak,virgin} - COD_{peak,virgin}\right)} \quad (5)$$

The index compares the crack-opening amplitude of the post peak interval for a stress decay equal to 15% of the peak strength, as in post-conditioning failure tests, to the amplitude featured by the reference virgin specimen for the same strength loss.

For specimens pre-cracked after the peak the same calculation is performed comparing the stress loss in a COD interval equal to 0.5 mm after the peak, that the same specimens features in the post-conditioning and in the pre-cracking regimes respectively (Figure 18b):

$$IDuR_{post\text{-}peak} = \frac{\left(f_{peak,\,post-conditioning} - \sigma_{0.5mm\ post-peak,\,post-conditioning}\right)}{\left(f_{peak,\,pre-cracking} - \sigma_{0.5mm\ post-peak,\,pre-cracking}\right)} \quad (6)$$

Results, though highlighting some recovery also of the post-peak ductility (Figurea 19 a-c), are actually quite sparse, even if a tendency to decrease, or at least remain unchanged upon prolonged immersion can be caught. Interestingly, comparing IDuR as well as $IDuR_{post\text{-}peak}$ to ISR (Figures 20a-b), the same sparsity with decreasing and/or invariable trend is obtained, whereas no recognizable trend between the two indices of ductility recovery has been achieved (Figure 20c).

3.3 Index of stiffness/damage recovery from mechanical 4pb tests

Thanks to unloading-reloading cycles performed both during pre-cracking and post-conditioning tests, the values of secant unloading and tangent reloading stiffness, respectively denoted as $K_{unl,j}$ and K_j, at different levels "j" of crack opening were evaluated (see Figure 21 for example). It is worth remarking that the unloading process always took place in a matter of few tenths of seconds, which is quite short for any significant relaxation to have occurred.

From them, an Index of Damage Recovery was calculated as:

Index of Damage Recovery IDaR= $\frac{K_{reloading,\,postconditioning} - K_{\text{unloading,pre-cracking}}}{K_{loading,\,pre-cracking} - K_{\text{unloading,pre-cracking}}}$ (7)

whose plots are shown in Figures 22 and 23a-c, respectively for deflection-softening and hardening specimens, and appear to be coherent with the previously discussed trends with reference to other indices. In particular:

- deflection softening specimens exhibited a stiffness recovery ranging from moderate to significant, as a function of exposure conditions, wet and dry cycles and exposure to open air providing the best results;
- all deflection-hardening specimens, except for old specimens, featured evident stiffness recovery, with influence of exposure conditions as expectable.

When correlated to other Indices of recovery of mechanical properties, IDaR seems to feature a same sign trend with ISR, but, coherently, a reverse sign one with IDuR (Figures 24 a-c). As a matter of fact, healing is likely to make specimens stronger and stiffer by restoring the material continuity at the cracked location, but at the same time, by likely increasing local bond and preventing further stress-redistribution upon reopening of the same cracks, also makes the same specimens somewhat less ductile.

3.4 Index of Toughness Recovery

For the sake of completeness, a recovery of the toughness for deflection-hardening specimens has been also calculated, by relating the area subtended by the post-conditioning nominal stress vs. COD curve up to 0.5 mm after the peak to the area subtended up to the same COD level by the curve of the reference virgin specimen (or, in the case of specimens pre-cracked beyond the peak, by the same specimen in the pre-cracking regime).

Results, in Figures 25 a-c, show a trend that, generally speaking, after an initial increase upon the first six months of exposure, remains thereafter constant or decreases. It is

anyway worth highlighting that in most cases the recovered performance attains levels comparable or even slightly higher that of the un-cracked reference specimens.

Effects of crack closures and of recovery of stress bearing capacity and ductility, as discussed above, can be called to explain the aforementioned trends, as also confirmed by correlation with indices of stress, ductility and damage recovery (Figures 26 a-d). Significantly, and coherently with previously exposed statements about the effects of crack-opening, the performance trends of specimens pre-cracked up to 2 mm or even beyond the peak, appear to be more stable than that of specimens pre-cracked at 1mm.

3.5 Index of stiffness/damage recovery from UPV test

In Figures 27a-b the values of the velocities are plotted, as measured in the central and edge portion of the specimen respectively, and in the three aforementioned testing stages, i.e. before pre-cracking, after pre-cracking and after conditioning.

It can be immediately observed that, for the data referring to the central part of the specimen, which undergoes cracking, a significantly slower wave is detected after cracking, followed, in case and as a function of the crack-opening and exposure conditions and durations, by recovery in the post-conditioning stage. On the other hand for the data referring to the edge portion of the specimen, no relevant change is detected neither between before and after pre-cracking, nor, more significantly, between after pre-cracking and after conditioning tests. This is likely to confirm that any measured recovery of the mechanical performance featured by the specimens, as extensively discussed above, is rightly attributable to the healing of the cracks and not, or at least not very significantly, to a delayed bulk hydration that the material may undergo along time, mainly when immersed in water or exposed to humid environments.

This, on the one hand, supported the reliability of the garnered results and of all the

analysis procedure explained and detailed so far and, on the other, makes it worthy to further process the UPV test data to obtain, from the measured wave speed velocities, an estimate of the stiffness/damage recovery defined as:

$$\text{Index of Damage Recovery } IDaR_{UPV} = \frac{UPV_{postconditioning} - UPV_{pre\text{-}cracking}}{UPV_{virgin} - UPV_{pre\text{-}cracking}} \quad (8)$$

The trends of the index as a function of the exposure conditions and times (Figures 28 a-d) are absolutely coherent with previously exposed comments, with reference to the Index of Damage Recovery as evaluated from mechanical 4 point bending tests.

Recovery, as estimated from destructive (4pb) and non-destructive (UPV) tests (Figure 29) also proves the reliability of the proposed experimental data processing procedures, with reference to the effects of crack sealing on the healing of different mechanical properties of the tested material.

3.6 Visual images and SEM analyses of healed cracks

Visual images of cracks featuring different healing degrees and for the different examined cases in terms of exposure conditions and durations and pre-crack openings are shown in Figure 30-35.

In order to support the analysis of experimental results performed so far, SEM analysis of the healed crack surfaces of selected specimens was performed after the final failure post-conditioning tests. In Figure 36 an example is shown of the fracture surface and of the composition of the healed products, in the case of a deflection softening specimen after 6 months in water. The composition of the products on the healed crack surfaces is absolutely coherent with products of delayed hydration of cement. For the sake of completeness and coherence, results of characterization of a siliceous grain sand on the fractured surface and of a fibre protruding from it are also shown.

4. Conclusions

In this paper the results have been presented and analysed in detail of a two year experimental program aimed at characterizing the autogenous self-healing capacity of High Performance Fibre-Reinforced Cementitious Composites (HPFRCCs) when exposed to different conditioning environments. Because of the effects of flow induced alignment of fibres, resulting in an either deflection-hardening or softening behaviour, different levels of crack openings were investigated.

The proposed methodology of analysis, which encompasses a wide range of parameters, including material behaviour, as above, crack-opening, exposure conditions and durations, may stand as a promising reference for the evaluation of self-healing capacity of advanced cement based materials in future research.

As from the analysis of the results presented in the paper, even if affected in some case by some scattering, it is evident that HPFRCCs feature a remarkable capacity of not merely sealing the cracks, but also of recovery their pristine level of mechanical performance in terms of load bearing capacity and stiffness. This capacity is obviously a function of the crack opening and of the exposure conditions and duration.

In general, presence of water, even in form of high air humidity or in the case of wet and dry cycles, favoured faster and higher healing. Moreover, prolonged exposure, even after two years, continued to induce healing, even if in some cases at a lower rate than in the early exposure times.

The healing results in terms of load bearing capacity and stiffness show an improvement of these properties, continuously growing with ongoing exposure even if to a different extent as a function of the exposure conditions. On the other hand, in terms of ductility, the recovery features a worsening trend with time of exposure. This can be explained by taking into account that self-healing products, restoring the material “cross-crack”

continuity and hence its “through-crack” load bearing capacity, also negatively affect, e.g. through some local bond increase, the transfer length and the consequent stress redistribution capacity which is responsible of ductility. As a matter of fact, upon post-conditioning tests, reopening of the previously formed cracks was always observed, and in no case a new crack formed at another location.

The autogenous self-healing capacity of HPFRCCs is primarily due to delayed hydration of un-hydrated cement and binder, resulting from high binder content and low water-to-binder ratios in the mix composition. Upon cracking, such products become exposed to outdoor moisture and/or water, which could not otherwise penetrate the quite impervious and compact skin of an undamaged specimen, and undergo delayed hydration reactions which produce CSH crystals sealing and healing the cracks. At the same time, fresh crack surfaces expose to outdoor environment, significantly to CO_2 in the air or dissolved in water, hydration products such as $Ca(OH)_2$ which may combine with carbon dioxide and produce $CaCO_3$ crystals also contributing to healing. The balance between the two aforementioned reactions is a function of exposure conditions and material composition and deserves further investigation also to understand the role of each process on the phenomenon of healing as well as of the recovery of the different investigated mechanical properties of the material. This has exceeded the scope of this paper.

In a forthcoming companion study, the data herein analysed will be complemented with visual microscopy and image analysis processing of crack closure, which will allow to quantitatively correlate the recovery of mechanical properties to the crack sealing.

The results obtained in this study hence contribute to define a new significance of the sustainability of structures made of or retrofitted with the signature category of cement based materials such as HPFRCCs, able to “rejuvenate” their physical and mechanical

performance upon cracking and thus to autogenously extend their service life. In a durability and sustainability based design framework the concept of "maximum healable crack width" (as a function of material compositions and structure service conditions, including stress level and environment exposure) could thus replace and/or "enrich" the current "absolute" crack opening threshold concepts.

Acknowledgments

The support of Politecnico di Milano – Young Researchers 2011 grant to the project Self-healing capacity of cementitious composites is gratefully acknowledged. The authors also thank Matteo Geminiani, Raffaele Gorlezza and Gregorio Sanchez Arevalo for their help in performing experimental tests along different time steps of the project, in partial fulfilment of the requirements to obtain their MScEng degrees.

References

[1] Mihashi, H. and Nishiwaki, T., Development of engineered self-healing and self-repairing concrete: state-of-the-art report, Journal of Advanced Concrete Technology, 10 (2012), 170-184.

[2] Van Tittelboom, K. and De Belie, N., Self-healing in cementitious materials – a review, Materials, 6 (2013), 2182-2217.

[3] Ferrara, L., Krelani, V. and Carsana, M., A fracture testing based approach to assess crack healing of concrete with and without crystalline admixtures, Construction and Building Materials, 68 (2014), 515-531.

[4] Roig-Flores, M., Moscato, S., Serna. P. and Ferrara, L., Self-healing capability of concrete with crystalline admixtures in different environments, Construction and Building Materials, 86 (2015), 1-11.

[5] Snoeck, D. and De Belie, N., From straw in bricks to modern use of microfibers in cementitious composites for improved autogeneous healing – A review, Construction and Building Materials, 95 (2015), 774-787.

[6] Vicenzino, E., Culham, G., Perry, V.H., Zakariasen, D and Chow, T.S., First use of UHPFRC in thin precast concrete roof shell for Canadian LRT station, PCI Journal (2005), 50-67.

[7] Jia, H.Y., Wei, C., Ming, X.Y. and Yang, E.H., The microstructure of self healed PVA ECC under wet and dry cycles, Materials Research, 13 (2010), 225-231.

[8] Sahmaran, M., Yildrim, G. and Erdem, T.K., Self-healing capability of cementitious composites incorporating different supplementary cementitious materials, Cement and Concrete Composites, 35 (2013), 89-101.

[9] Sahmaran, M., Yildrim, G., Noori, R., Ozbay, E. and Lachemi, M., Repeatability and pervasiveness of self healing in engineered cementitious composites, ACI Materials Journal, 112 (2015), 513-522.

[10] Hannant, D. J. and Keer, J. G., Autogenous healing of thin cement based sheets, Cement and Concrete Research, 13 (1983), 357–365.

[11] Gray R. J. and Shear, B., Autogeneous healing of fibre/matrix interfacial bond in fibre-reinforced mortar, Cement and Concrete Research, 14 (1984), 315–317.

[12] Homma, D., Mihashi, H. and Nishiwaki, T., Self-Healing Capability of Fibre Reinforced Cementitious Composites, Journal of Advanced Concrete Technology, 7 (2009), 217–228.

[13] Yang, Y., Lepech, M. D., Yang, E.-H. and Li, V. C., Autogenous healing of engineered cementitious composites under wet–dry cycles, Cement and Concrete Research, 39 (2009), 382–390.

[14] Li, M. and Li, V.C., Cracking and healing of engineered cementitious

composites under chloride environment, ACI Materials Journal, 108 (2011), 333-340.

[15] Yang, Y., Yang, E.H. and Li, V.C., Autogenous healing of engineered cementitious composites at early ages, Cement and Concrete Research, 41 (2011), 176-183.

[16] Snoeck, D., Van Tittelboom, K., Steuperaert, S., Dubruel. P. and De Belie, N., Self-healing cementitious materials by the combination of microfibers and superabsorbent polymers, Intelligent Material Systems and Structures, 25 (2014), 13-24.

[17] Snoeck, D. and De Belie, N., Repeated autogenous healing in strain-hardening cementitious composites by using superabsorbent polymers, ASCE Journal of Materials in Civil Engineering, (2015) DOI 10.1061/(ASCE)MT.1943-5533.0001360.

[18] Ferrara, L., Crystalline admixtures in cementitious composites: from porosity reducers to catalysts of self-healing, in V. Mechtcherine and C. Schroefl, eds., Proceedings International Conference on Application of SAP and new admixtures in concrete construction, Dresden, Germany, Sept. 14-17 2014, RILEM Pubs., 311-324.

[19] De Rooij, M.R., Qian, S., Liu, H., Gard, W.F. and van de Kuilen, J.W.G., Using natural wood fibers to self-heal concrete, in M.G. Alexander et al., eds., Proceedings 2nd international Conference on Concrete Repairing, Rehabilitation and Retrofitting, Cape Town, 24-26 Nov. 2008, Taylor and Francis, London, 229-234.

[20] Snoeck, D. and De Belie, N., Mechanical and self-healing properties of cementitious composites reinforced with flax and cottonised flax and compared with polyvinyl alcohol fibres, Biosystems Engineering, 111 (2012), 325-335.

[21] Ferrara, L., Ferreira, S.R., Krelani, V., Silva, F. and Toledo Filho, R.D., Effect of natural fibres on the self healing capacity of high performance fibre reinforced cementitious composites, in E. Schlangen et al., eds., Proceedings SHCC3, 3rd international RILEM conference on strain hardening cementitious composites,

Dordrecht, The Netherlands, 3-5 Nov, 2014, RILEM Pubs., 9-16.

[22] Ferrara L., Ferreira, S.R., Krelani, V., Della Torre, M., Silva, F. and Toledo Filho, R.D., Natural fibres as promoters of autogenous healing in HPFRCCs: results from an on-going Italy-Brasil cooperation, in M.A. Chiorino et al., eds., ACI Special Publication 305. DSCS – Workshop Proceedings, Bologna, Italy, 1-3 Oct. 1-3 2015.

[23] Ferrara, L., Ozyurt, N. and di Prisco, M., High mechanical performance of FRCCs: the role of "casting-flow" induced fiber orientation, Materials and Structures, 44 (2011), 109-128.

[24] Ferrara, L., Krelani, V. and Moretti, F., Autogenous healing on the recovery of mechanical performance of HPFRCCs: part 2 – correlation between healing of mechanical performance and crack sealing, in preparation.

[25] Ferrara, L., Faifer, M. and Toscani, S., A magnetic method for non destructive monitoring of fiber dispersion and orientation in Steel Fiber Reinforced Cementitious Composites – part 1: method calibration, Materials and Structures, 45 (2012), 575-589.

[26] Ferrara, L., Faifer, M., Muhaxheri, M. and Toscani, S., A magnetic method for non destructive monitoring of fiber dispersion and orientation in Steel Fiber Reinforced Cementitious Composites – part 2: correlation to tensile fracture toughness, Materials and Structures, 45 (2012), 591-598.

[27] di Prisco, M., Ferrara, L. and Lamperti, M.G.L., Double Edge Wedge Splitting (DEWS): an indirect tension test to identify post-cracking behaviour of fibre reinforced cementitious composites, Materials and Structures, 46 (2013), 1893-1918.

[28] Ferrara, L., Tailoring the orientation of fibers in High Performance Fiber Reinforced Cementitious Composites: part 1 - experimental evidence, monitoring and prediction, Journal of Materials and Structures Integrity, 9 (2015), 72-91.

[29] Ferrara, L., Tailoring the orientation of fibers in High Performance Fiber

Reinforced Cementitious Composites: part 2 - correlation to mechanical properties and design implications, Journal of Materials and Structures Integrity, 9 (2015), 92-107.

Notation

$f_{peak,pre\text{-}cracking}$ **:** maximum nominal bending stress in the pre-cracking test

$f_{peak,post\text{-}conditioning}$ **:** maximum nominal bending stress in the post-conditioning test

$f_{peak,virgin}$ **:** maximum nominal bending stress of the virgin reference specimen tested monotonically up to failure

$\sigma_{N,unloading,\ pre\text{-}cracking}$**:** nominal bending stress of the specimen at the Crack Opening Displacement (COD) level attained during pre-cracking (before unloading the specimen for condition treatment)

$\sigma_{N,unloading,\ virgin}$**:** nominal bending stress of the virgin reference specimen at the same COD level attained during pre-cracking tests for companion specimens

$\sigma_{N,0.5\ mm\ DP\ pre\text{-}cracking}$**:** nominal bending stress during the pre-cracking test at a COD value equal to 0.5 mm after the peak (only for specimens pre-cracked beyond the peak)

$\sigma_{N,0.5\ mm\ DP\ post\text{-}conditioning}$**:** nominal bending stress during the post-conditioning test at a COD value equal to 0.5 mm after the peak (only for specimens pre-cracked beyond the peak)

$COD_{1st\ crack,\ pre\text{-}cracking}$**:** COD at 1st cracking during the pre-cracking test

$COD_{1st\ crack,\ pre\text{-}cracking}$**:** COD at 1st cracking during the pre-cracking test

$COD_{1st\ crack,\ virgin}$**:** COD at 1st cracking of the virgin reference specimen tested monotonically up to failure

$COD_{peak,\ pre\text{-}cracking}$**:** COD at the maximum nominal bending stress during the pre-cracking test (only for specimens pre-cracked beyond the peak)

$COD_{peak,\ post\text{-}conditioning}$**:** COD at at the maximum nominal bending stress during the post-conditioning test

$COD_{peak,\ virgin}$**:** COD at the maximum nominal bending stress exhibited by the reference virgin specimen tested monotonically up to failure

$COD_{unloading,\ pre\text{-}cracking}$**:** maximum value of the COD attained during the pre-cracking tests, upon which attainment the specimen was unloaded and exposed to conditioning

$COD_{85\%\ fpeak,pre\text{-}cracking}$**:** COD value measured during the pre-cracking test in the post-peak softening regime corresponding to a stress value equal to 85% of the peak stress (only for deflection hardening specimens pre-cracked beyond the peak)

$COD_{85\%\ fpeak,post\text{-}conditioning}$**:** COD value measured during the post-conditioning test in the post-peak softening regime corresponding to a stress value equal to 85% of the peak stress (only for deflection hardening specimens pre-cracked beyond the peak)

$K_{loading,pre\text{-}crack}$**:** tangent stiffness measured when loading the specimen during the pre-cracking test

$K_{reloading,post\text{-}conditioning}$**:** tangent stiffness measured when reloading the specimen in the post-conditioning test

$K_{unloading,pre\text{-}crack}$**:** secant stiffness measured when un-loading the specimen in the pre-cracking test, upon attainment of the maximum prescribed pre-crack opening

Tables

Table 1. Mix-design of HPFRCC

Constituent	Dosage (kg/m^3)
Cement	600
Slag	500
Sand (0-2 mm)	982
Water	200
Superplasticizer	33 (l/m^3)
Straight steel fibres (l_f = 13 mm; d_f = 0.16 mm)	100

Table 2.

		Deflection behaviour											
		Softening			**Hardening**								
Pre-crack opening		**0.5 mm**			**1 mm**			**2 mm**			**COD_{peak} + 0.5 mm**		
Exposure duration (months)		**1**	**6**	**24**	**1**	**6**	**24**	**1**	**6**	**24**	**1**	**6**	**24**
Exposure Conditions	**Water immersion**	*1*	*2*	*1*	*1*	*1*	*1*	*2*	*1*	*2*	*2*	*2*	*2*
	Air exposure	*1*	*2*	*1*	*1*	*1*	*1*	*2*	*1*	*2*	*2*	*2*	*1*
	20°C – RH = 90%	*1*	*2*	*1*	*1*	*1*	*1*	*2*	*1*	*2*	*2*	*2*	*2*
	20°C – RH = 50%	*1*	*=*	*2*	*1*	*1*	*1*	*2*	*4*	*2*	*2*	*2*	*2*
	Wet and dry	*1*	*2*	*2*	*1*	*1*	*1*	*2*	*2*	*1*	*2*	*2*	*2*

Synopsis of the experimental program: number of specimens tested per each exposure condition and duration, deflection hardening/softening behaviour and pre-crack opening (**Age of pre-crack of 2 months**)

		Deflection behaviour															
		Softening				**Hardening**											
Pre-crack opening		**0.5 mm**				**1 mm**				**2 mm**				**COD_{peak} + 0.5 mm**			
Exposure duration (months)		**1**	**3**	**6**	**24**	**1**	**3**	**6**	**24**	**1**	**3**	**6**	**24**	**1**	**3**	**6**	**24**
Age of pre-crack	**2 months**	*1*		*2*	*1*	*1*		*1*	*1*	*2*		*1*	*2*	*2*		*2*	*2*
	11 months	*3*	*2*	*3*		*1*	*1*	*=*		*1*	*1*	*1*		*1*	*1*	*1*	

Synopsis of the experimental program: number of specimens tested per each exposure duration, age of pre-cracking, deflection hardening/softening behaviour and pre-crack opening (**Exposure Conditions Water immersion**)

Figures

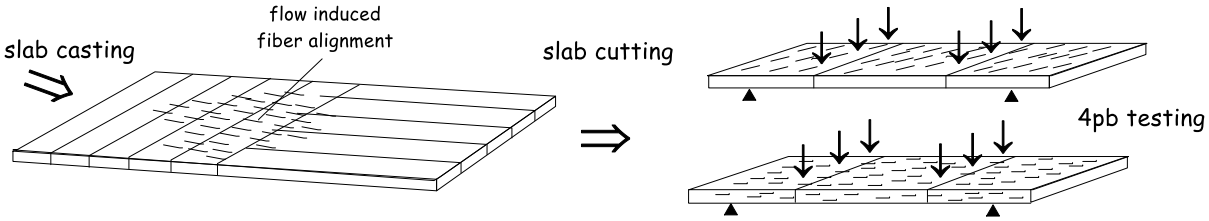

Figure 1. Slab casting scheme and beam specimen cutting procedure

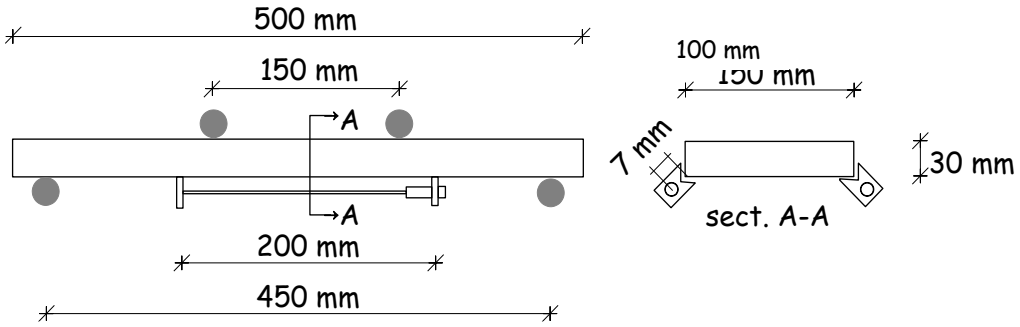

Figure 2. 4-point bending tests set-up for beam specimens obtained as in Figure 1.

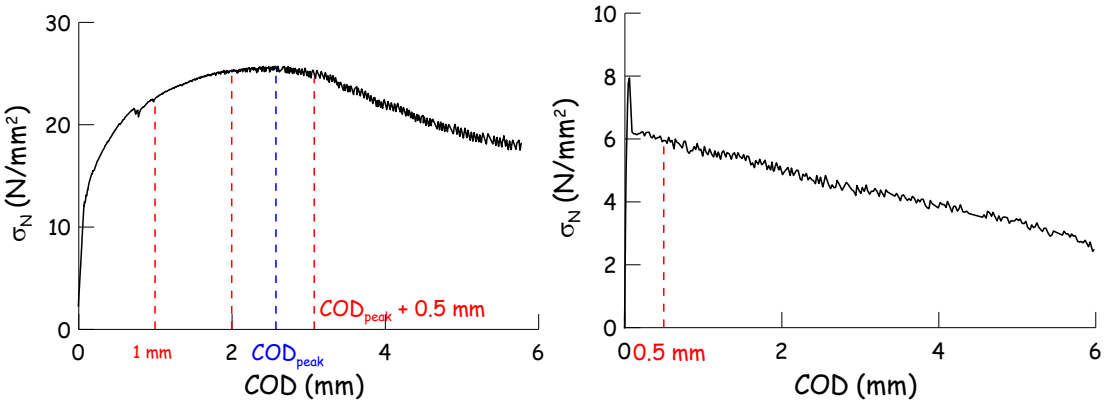

(a) (b)

Figure 3. Nominal stress σ_N vs. COD curves for specimens featuring: (a) stable pre-peak multi-cracking and deflection hardening behaviour (fibres parallel to the bending axis); (b) unstable post-cracking localization and deflection softening behaviour (fibres orthogonal to the bending axis).

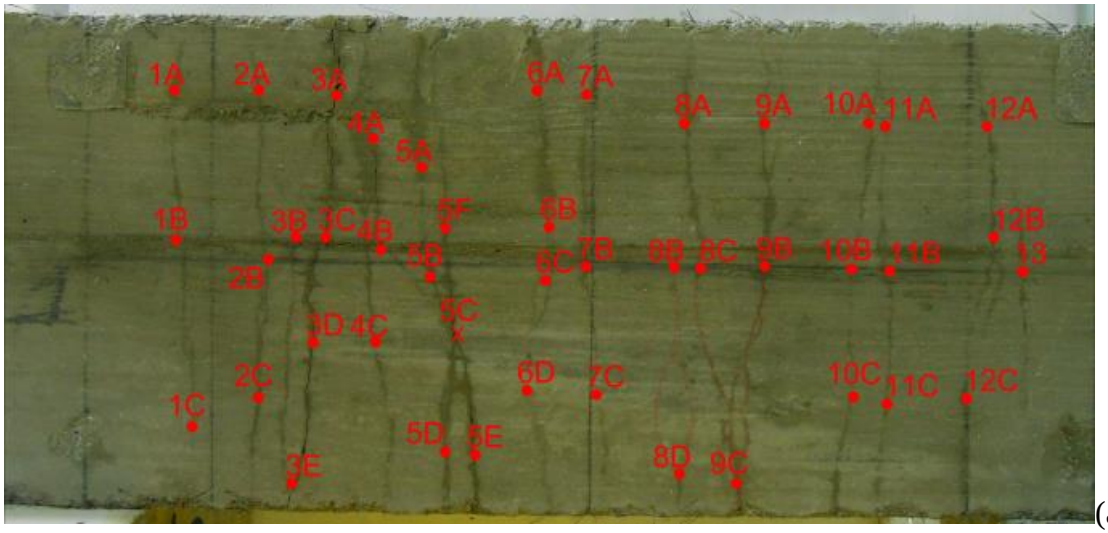

(a)

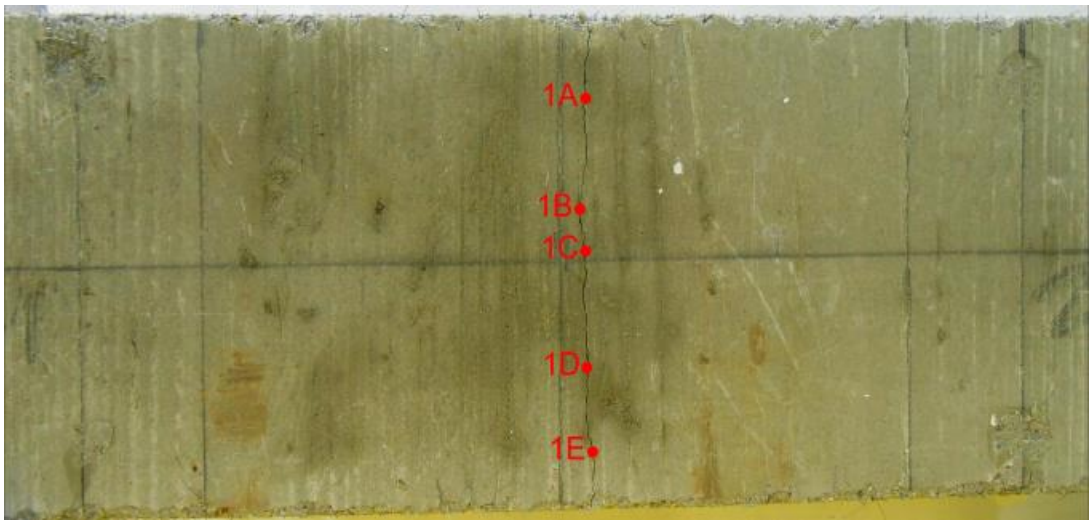

(b)

Figure 4. Crack patterns in specimens featuring: (a) stable pre-peak multi-cracking and deflection hardening behaviour (curve in Figure 3a); (b) unstable post-cracking localization and deflection softening behaviour (curve in Figure 3b).

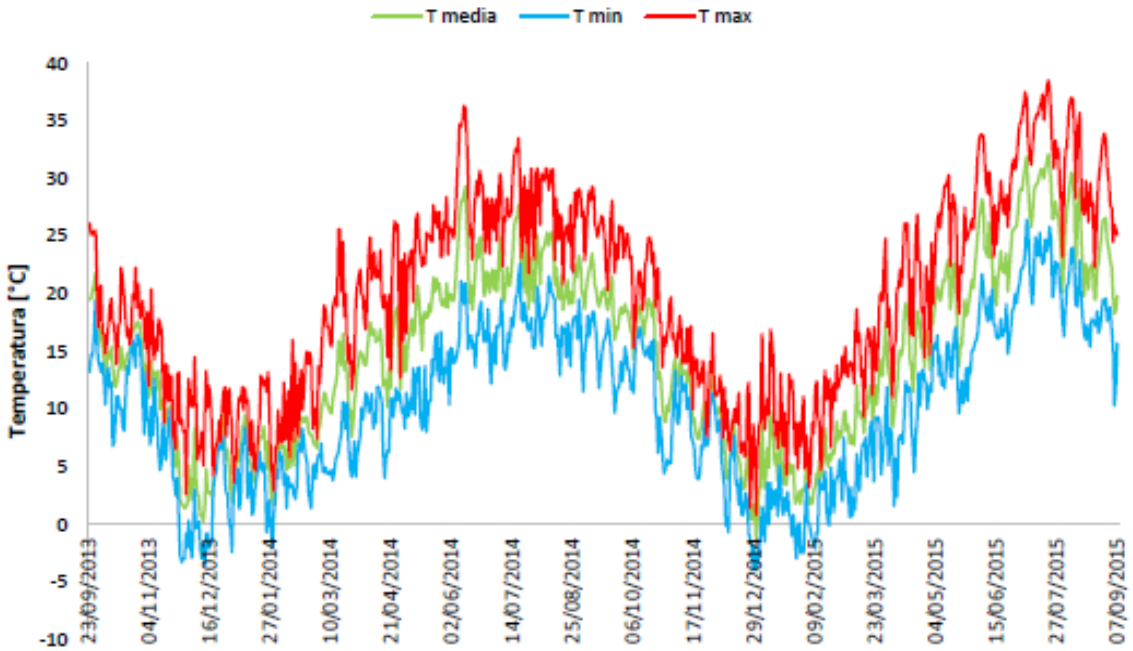

(a)

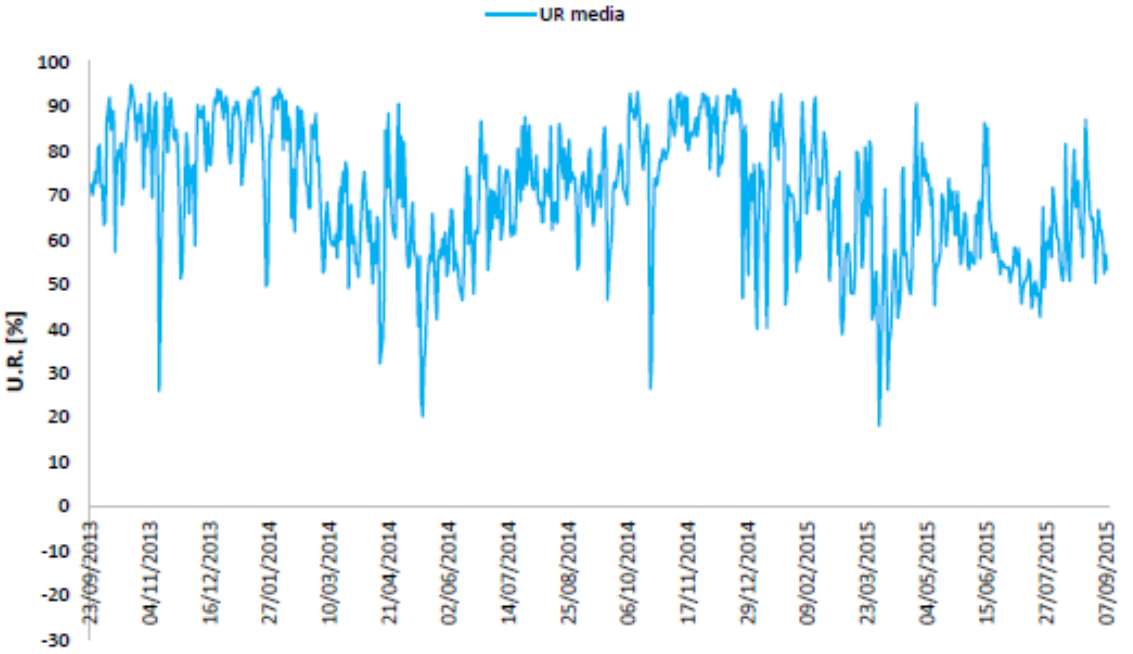

(b)

Figure 5: trends of average and minimum and maximum temperatures (a) and of relative humidity (b) in Milan all along the exposure time of specimens

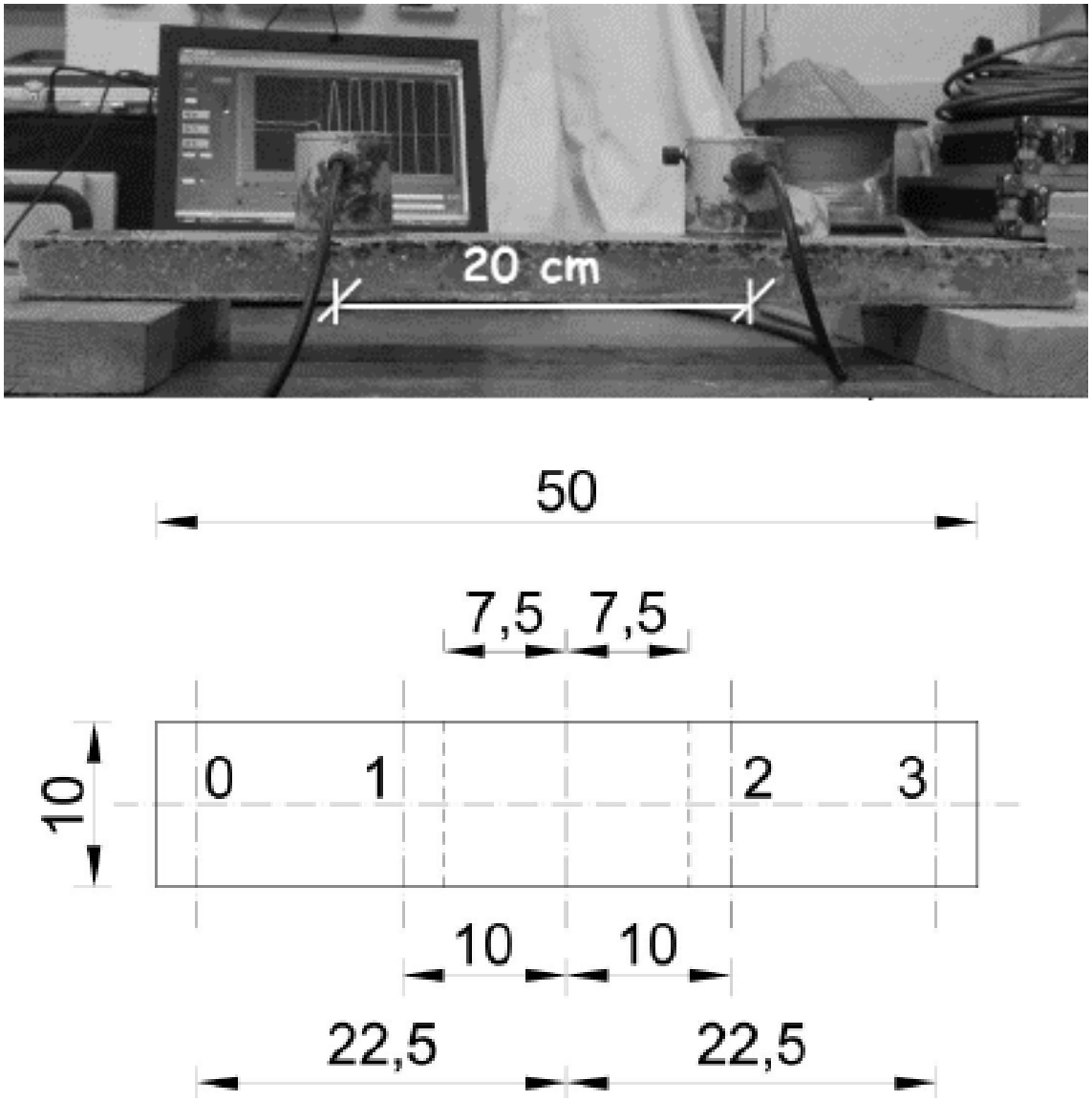

Figure 6. Ultrasonic Pulse Velocity test set-up (a) and schematic of the reference positions or UPV measurements (b): references 0 and 3 will be supports during testing whereas the zone between references 1 and 2 will undergo cracking because of the applied bending moment – measurements have been taken in zone 0-1 (for undamaged reference) and 1-2 (for cracked portion of the specimen) – measures in cm.

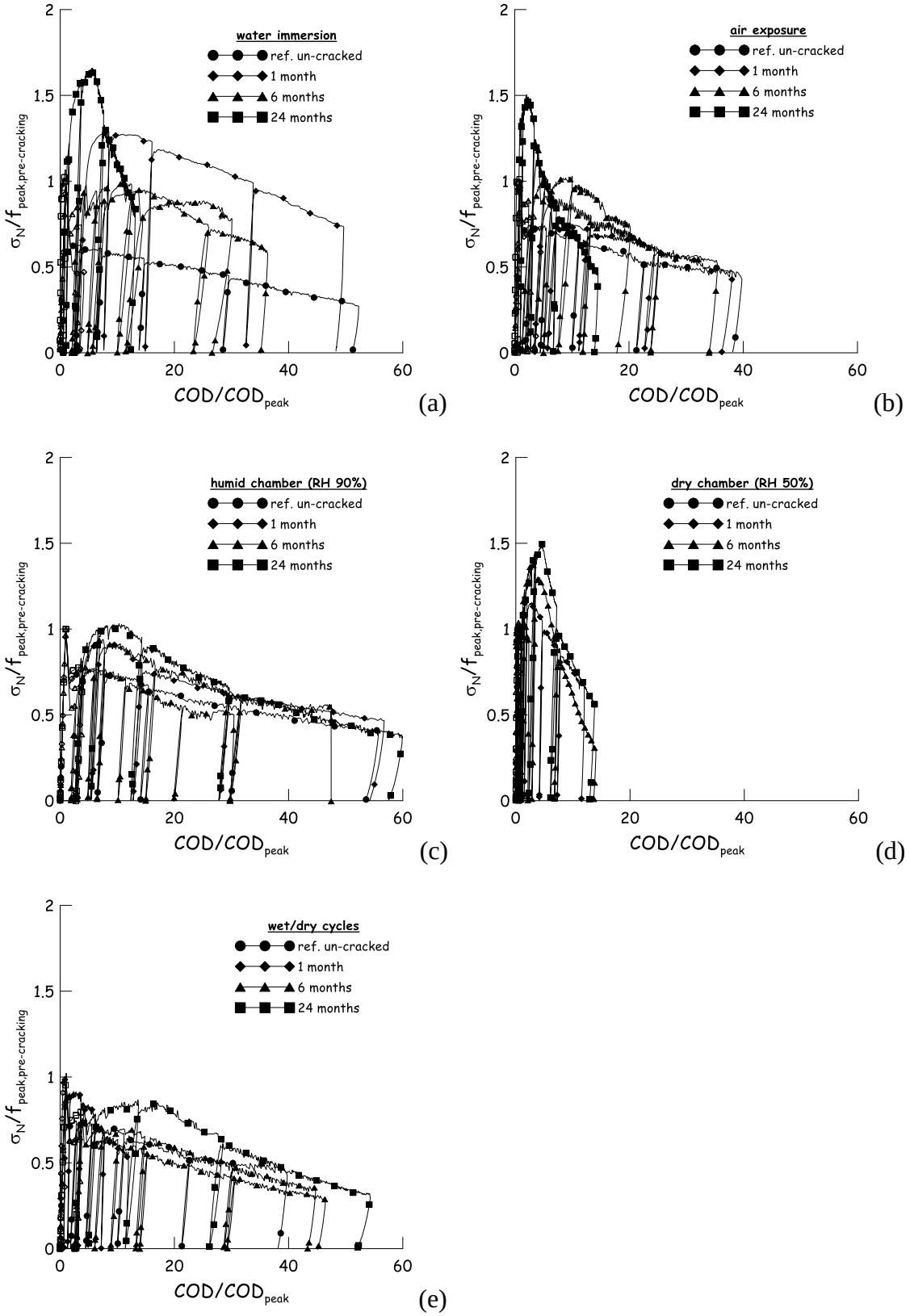

Figure 7. σ_N vs. COD curves in pre-cracking (2 months) and post-conditioning regimes - deflection softening specimens and conditioned under water (a), air exposure (b), RH 90% (c) and RH 50% room (d) and wet-dry cycles.

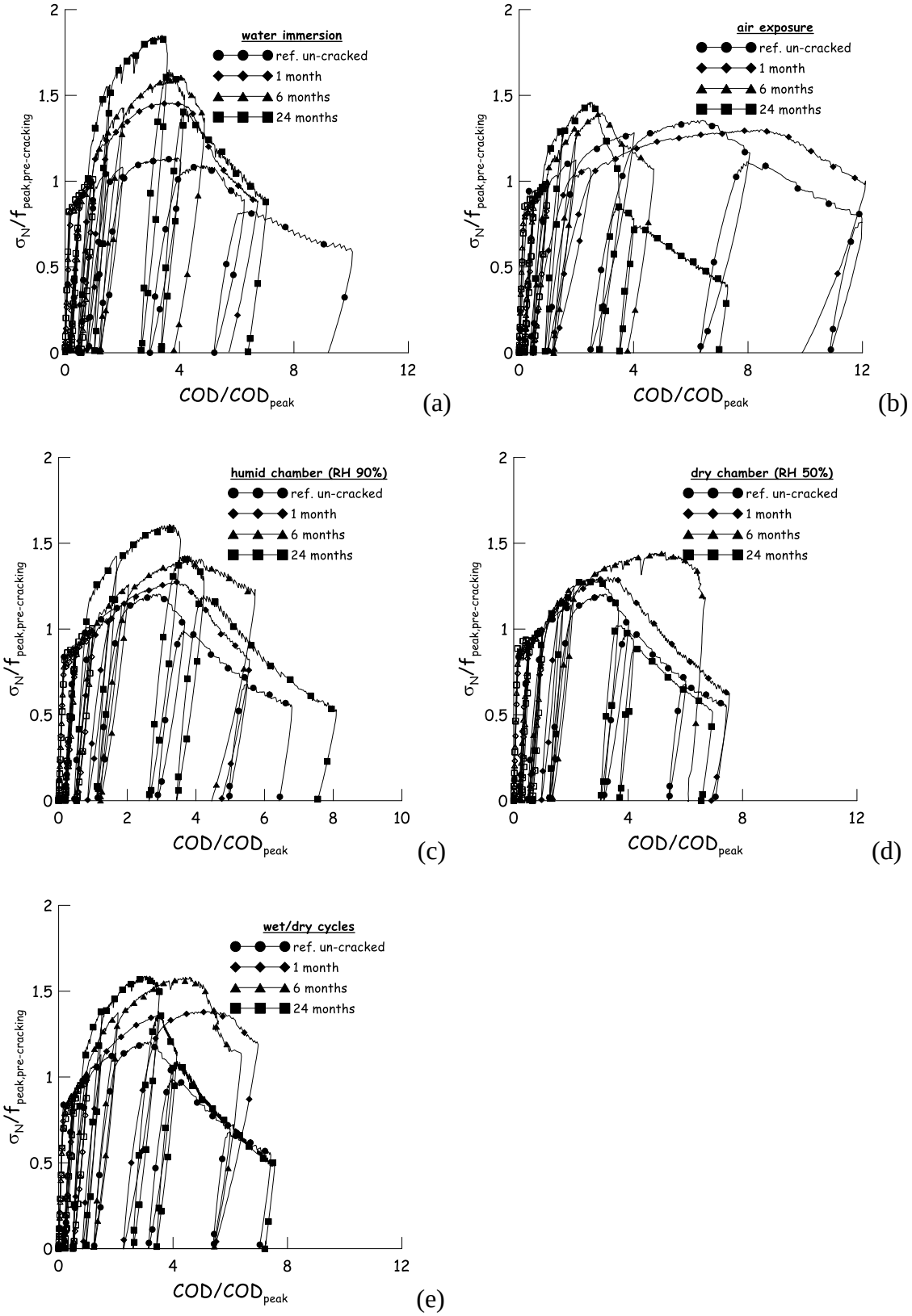

Figure 8. σ_N vs. COD curves in pre-cracking (2 months) and post-conditioning regimes - deflection hardening specimens pre-cracked at 1 mm and conditioned under water (a), air exposure (b), RH 90% (c) and RH 50% room (d) and wet-dry cycles (e).

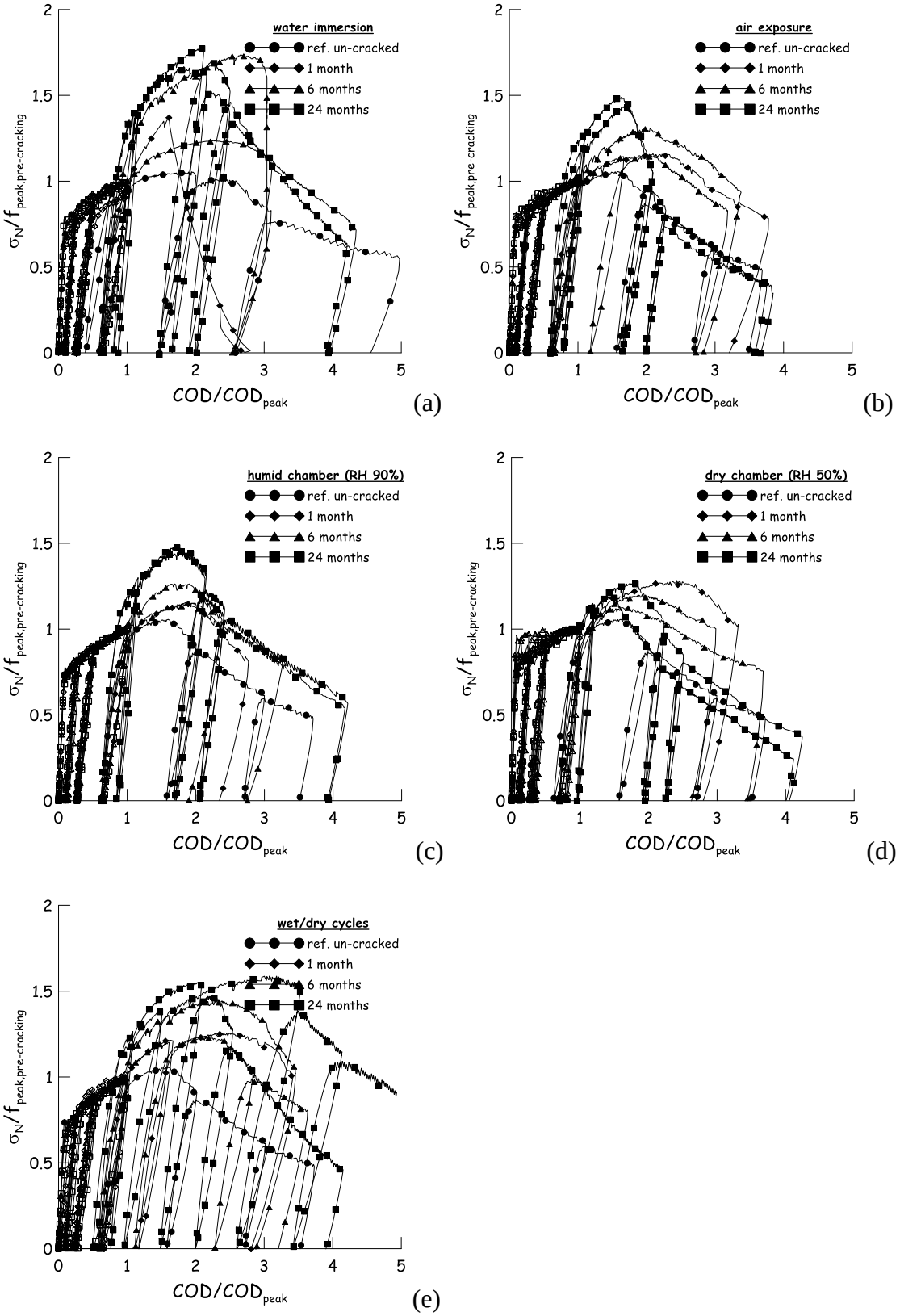

Figure 9. σ_N vs. COD curves in pre-cracking (2 months) and post-conditioning regimes - deflection hardening specimens pre-cracked at 2 mm and conditioned under water (a), air exposure (b), RH 90% (c) and RH 50% room (d) and wet-dry cycles (e).

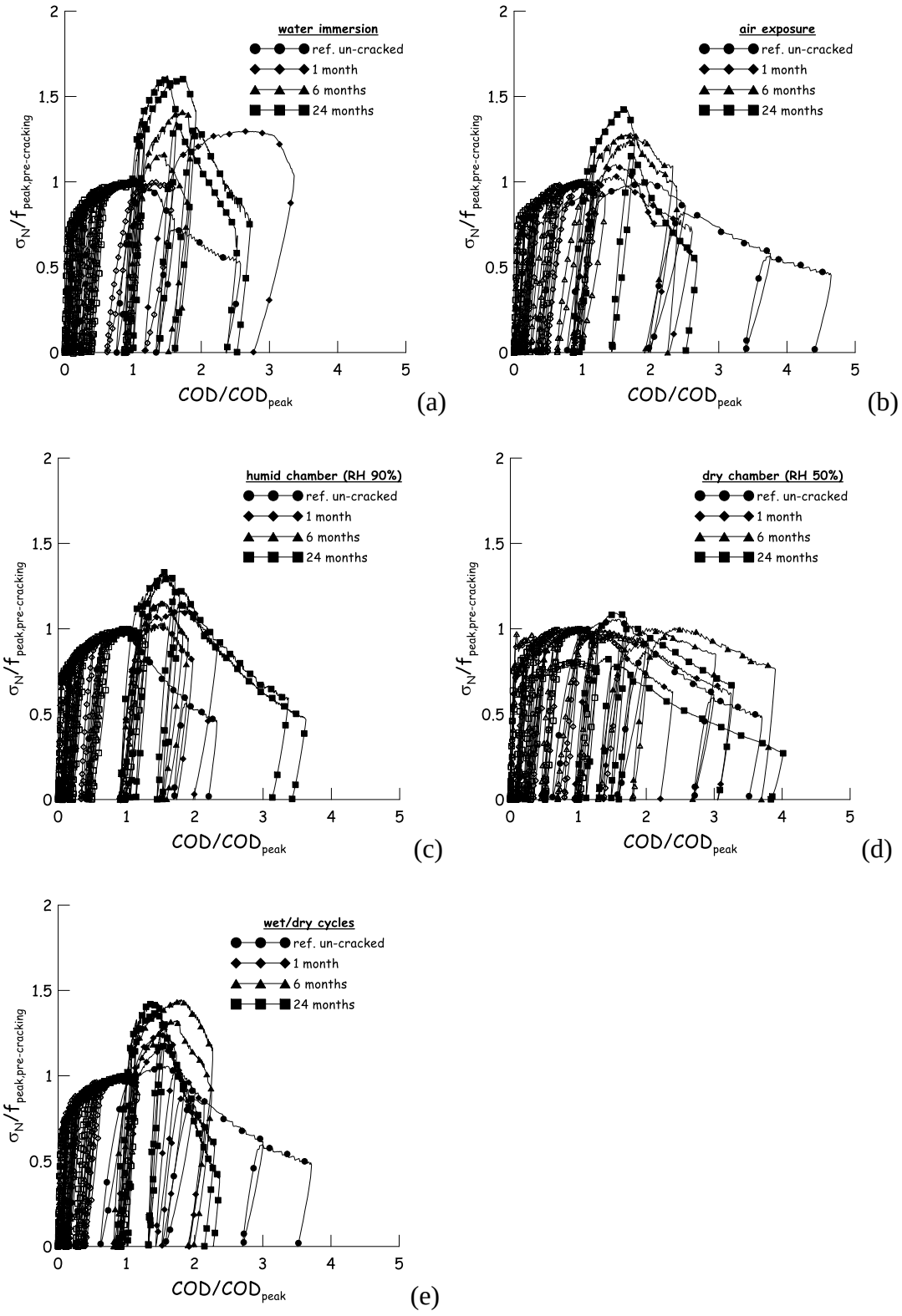

Figure 10. σ_N vs. COD curves in pre-cracking (2 months) and post-conditioning regimes -deflection hardening specimens pre-cracked at COD_{peak}+0.5 mm and conditioned under water (a), air exposure (b), RH 90% (c) and RH 50% room (d) and wet-dry cycles (e).

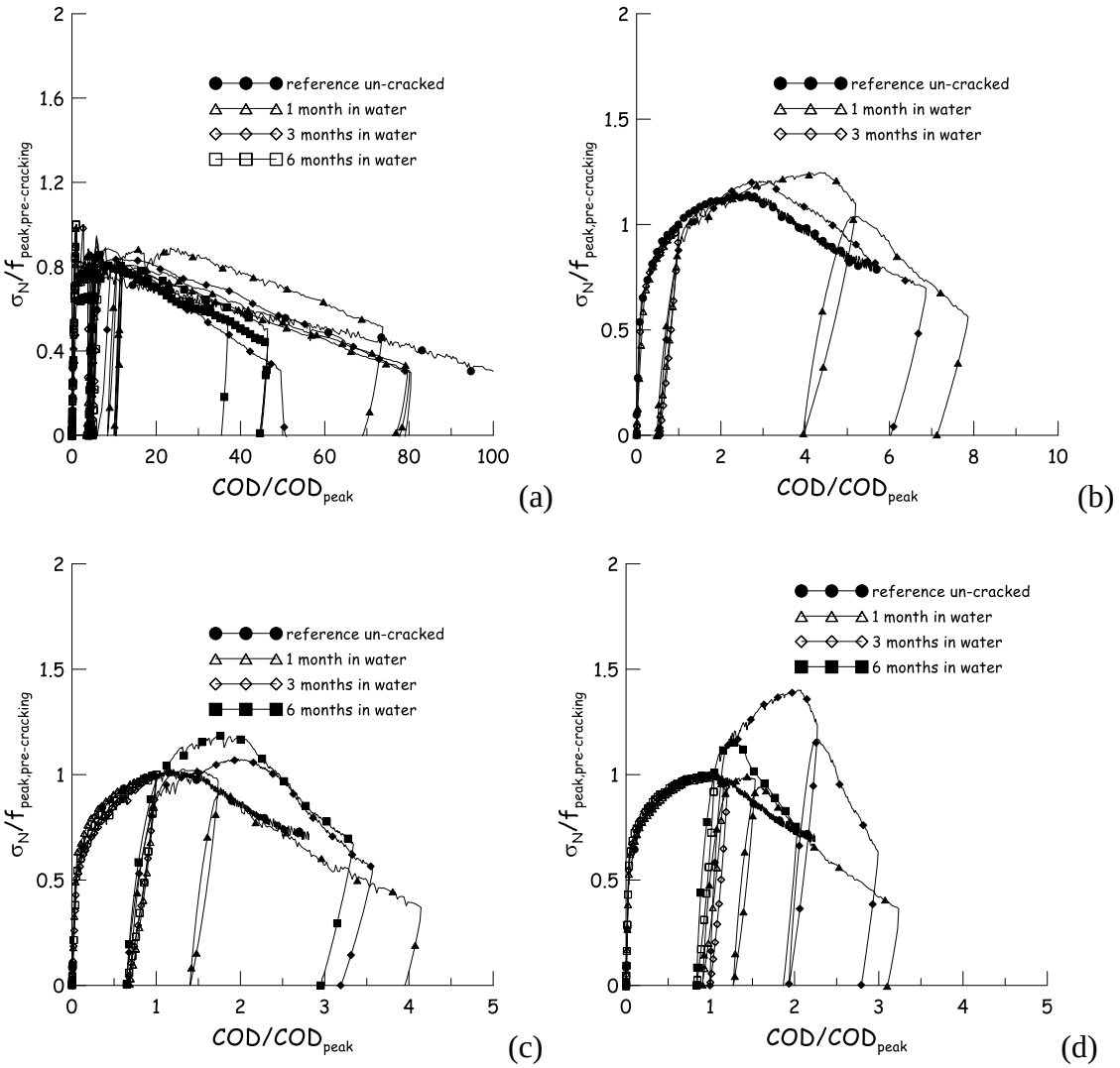

Figure 11. σ_N vs. COD curves in pre-cracking (11 months) and post-conditioning regimes – deflection softening (a) and deflection hardening specimens pre-cracked at 1 mm (b), 2 mm (c) and COD_{peak}+0.5 mm (d) and conditioned under water.

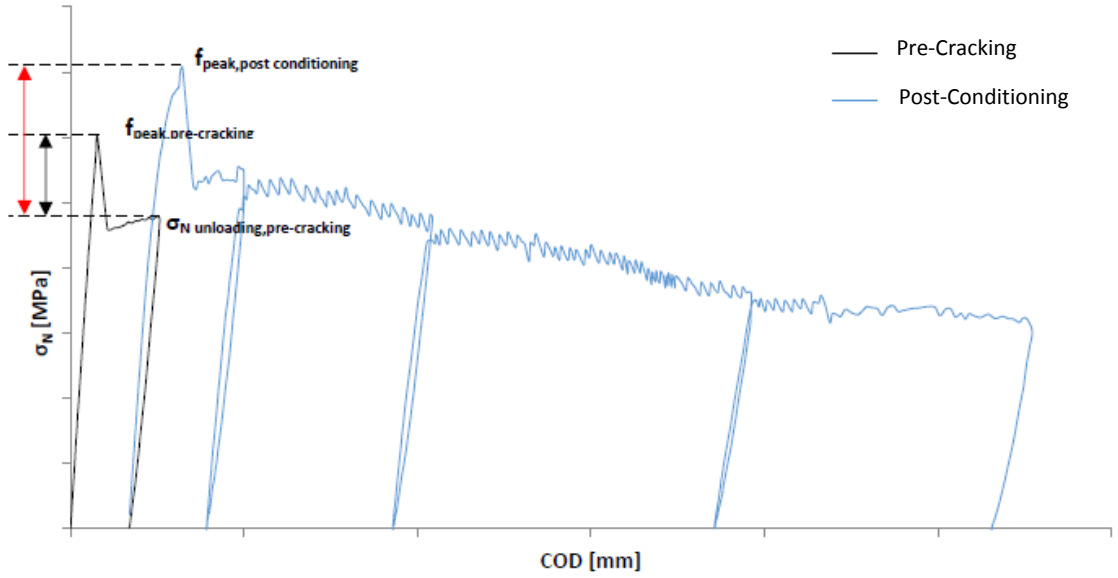

Figure 12. Notation and definition of the parameters for the Index of Strength Recovery for deflection-softening specimens.

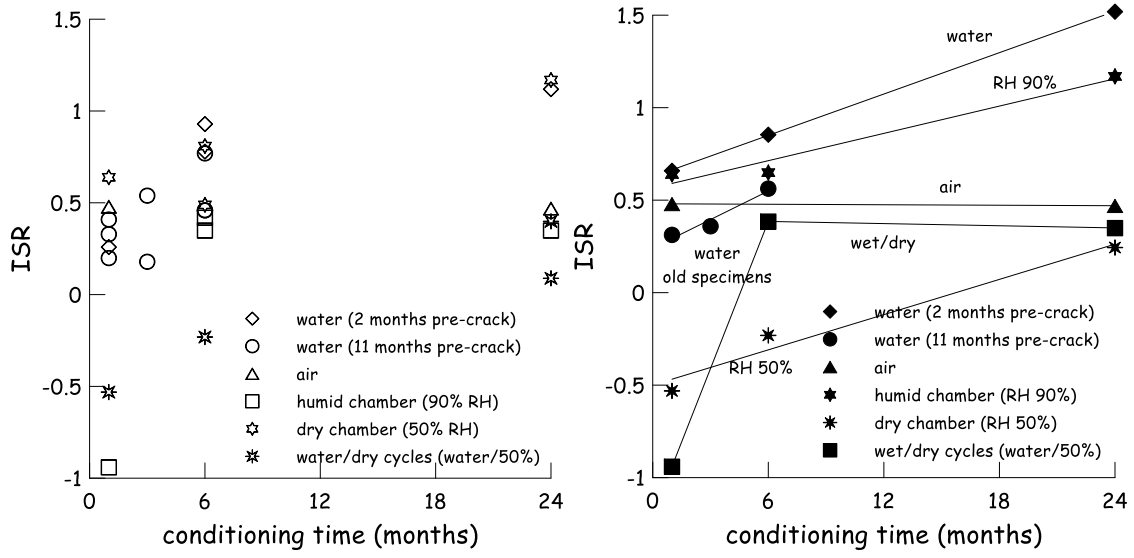

(a) (b)

Figure 13. Index of Strength Recovery vs. conditioning time for deflection softening specimens (hollow markers refer to values of single tests (a), solid markers represent average values of nominally identical tests (b)).

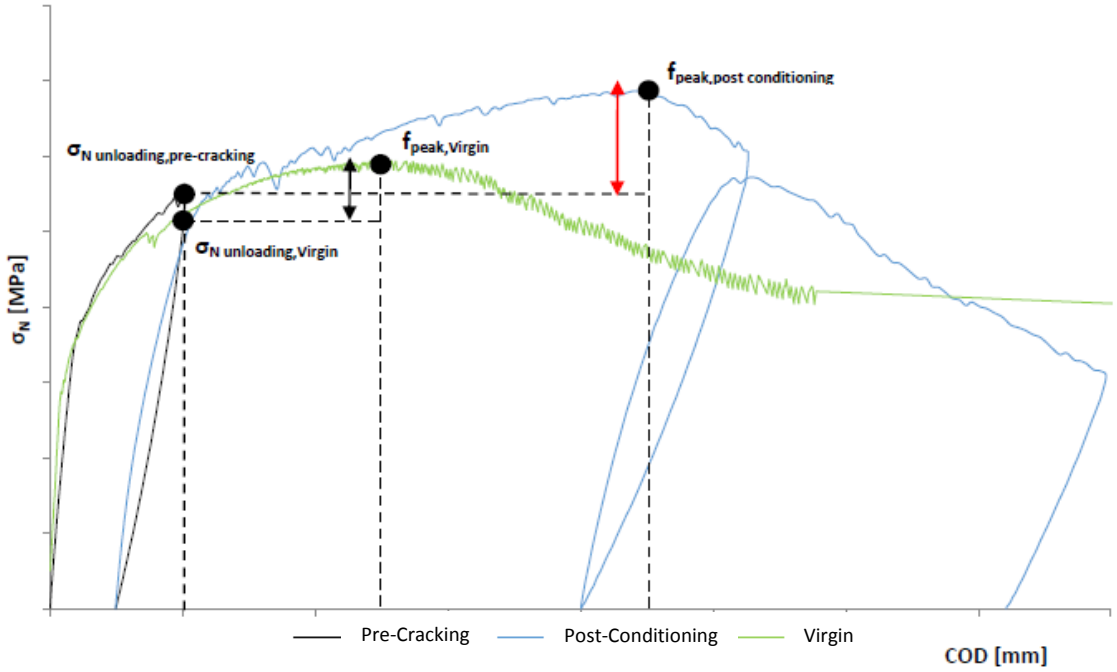

(a)

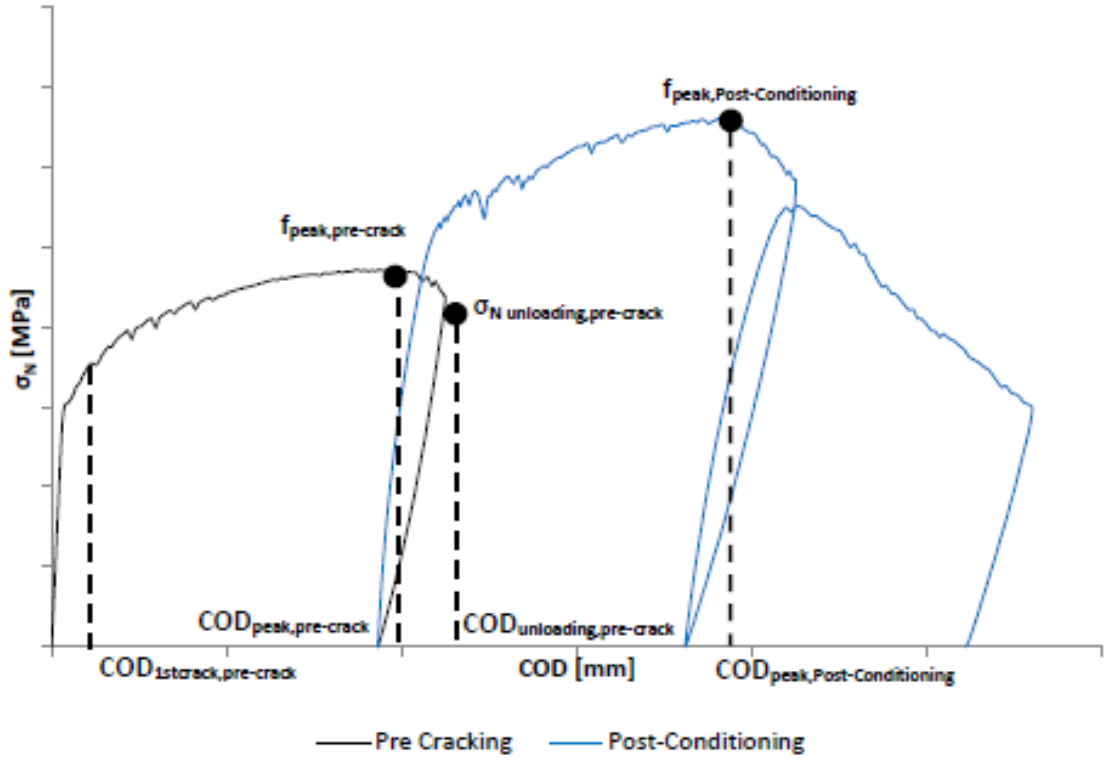

(b)

Figure 14. Definition of parameters to calculate the Index of Strength Recovery for deflection-hardening specimens pre-cracked in pre-peak (a) and post-peak regime (b).

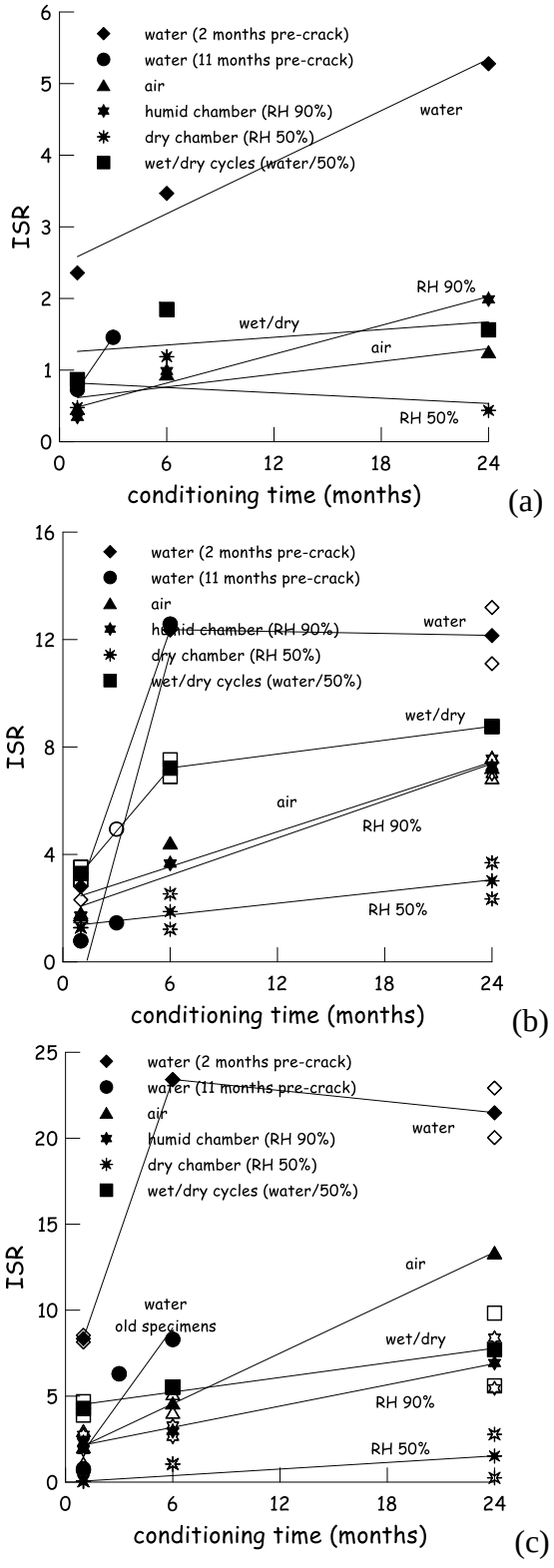

Figure 15. Index of Strength Recovery vs. conditioning time for deflection-hardening specimens pre-cracked up to 1 mm (a), 2 mm(b) and 0.5 mm after the peak (c) (hollow markers refer to values of single tests, solid markers represent average values of nominally identical tests).

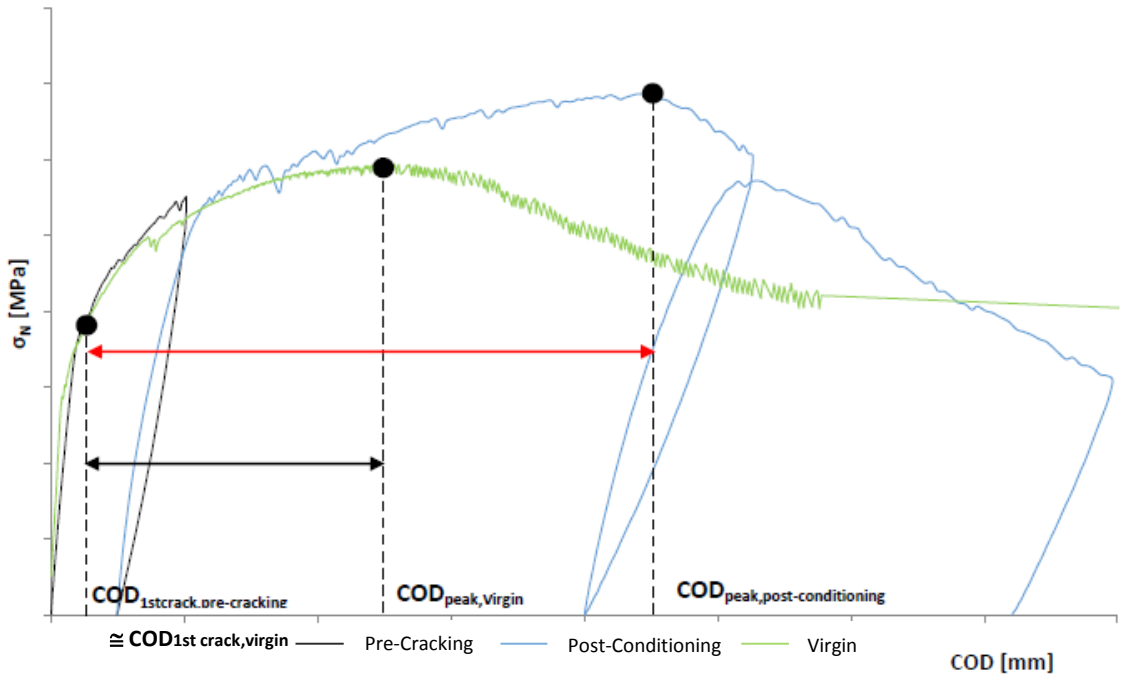

(a)

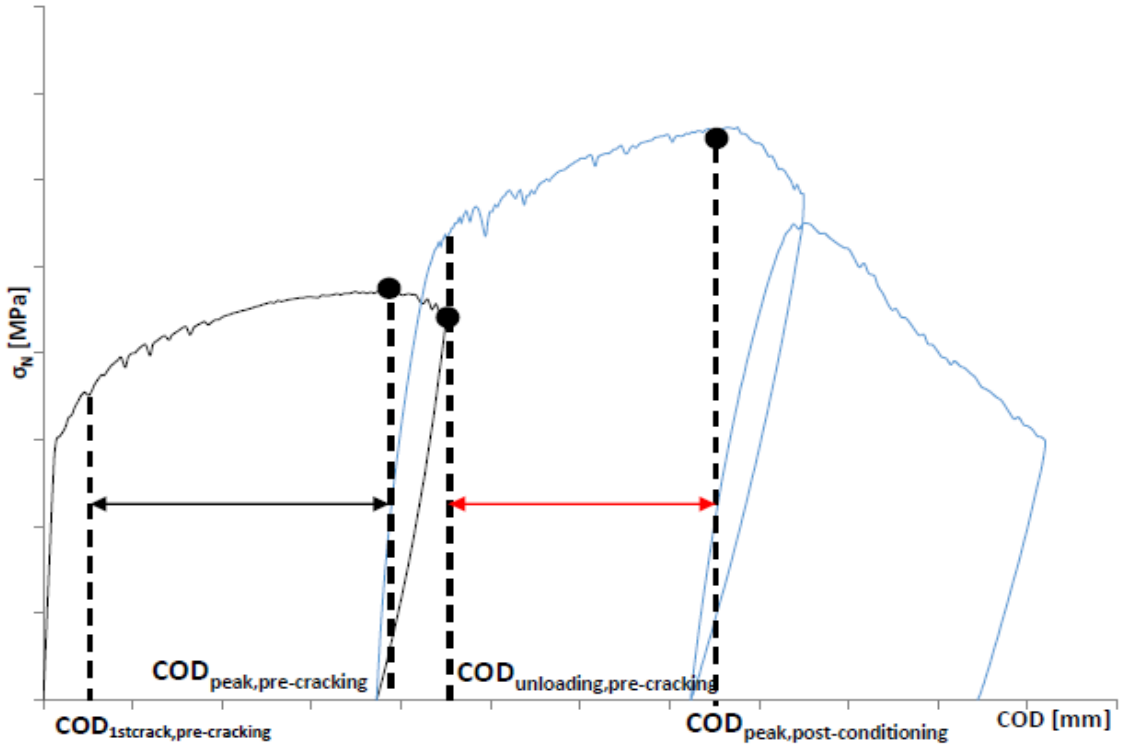

(b)

Figure 16. Notation and definition of the parameters for the Index of Ductility Recovery for deflection-hardening specimens pre-cracked in the pre-peak (a) and post-peak regime (b).

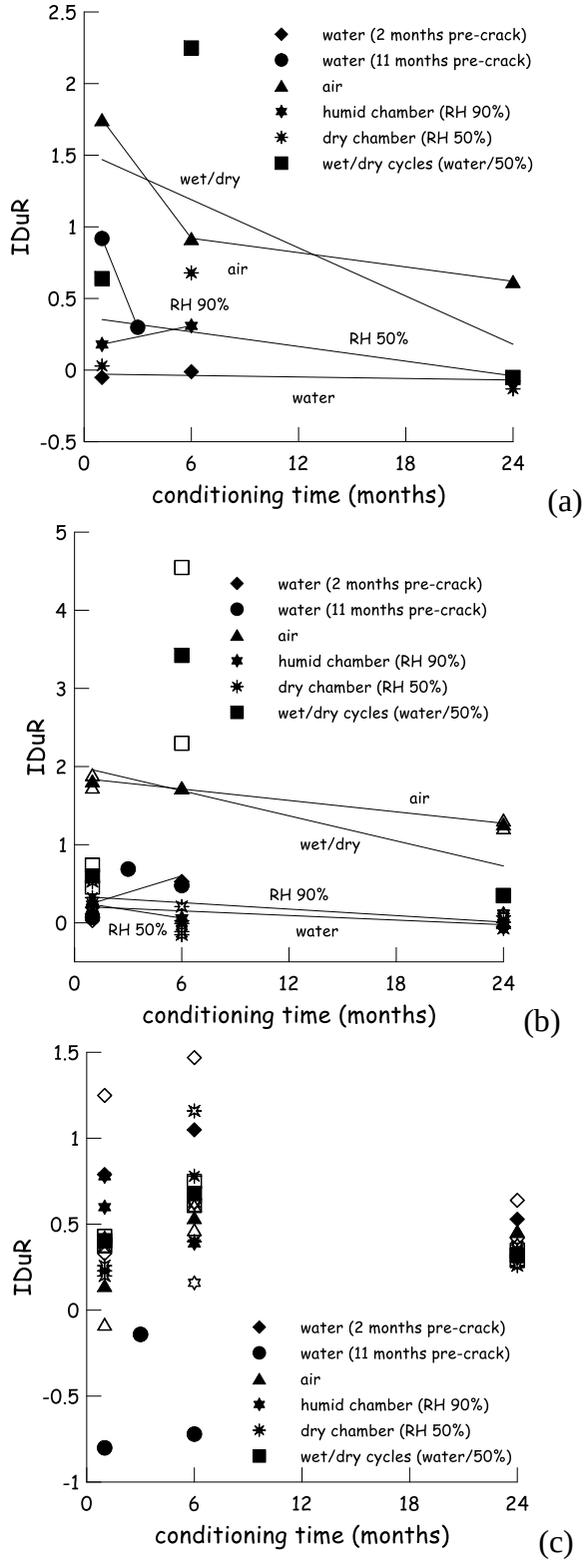

Figure 17. Index of Ductility Recovery (peak) vs. conditioning time for deflection hardening specimens pre-cracked up to 1 mm (a), 2 mm(b) and 0.5 mm after the peak (c) (hollow markers refer to values of single tests, solid markers represent average values of nominally identical tests).

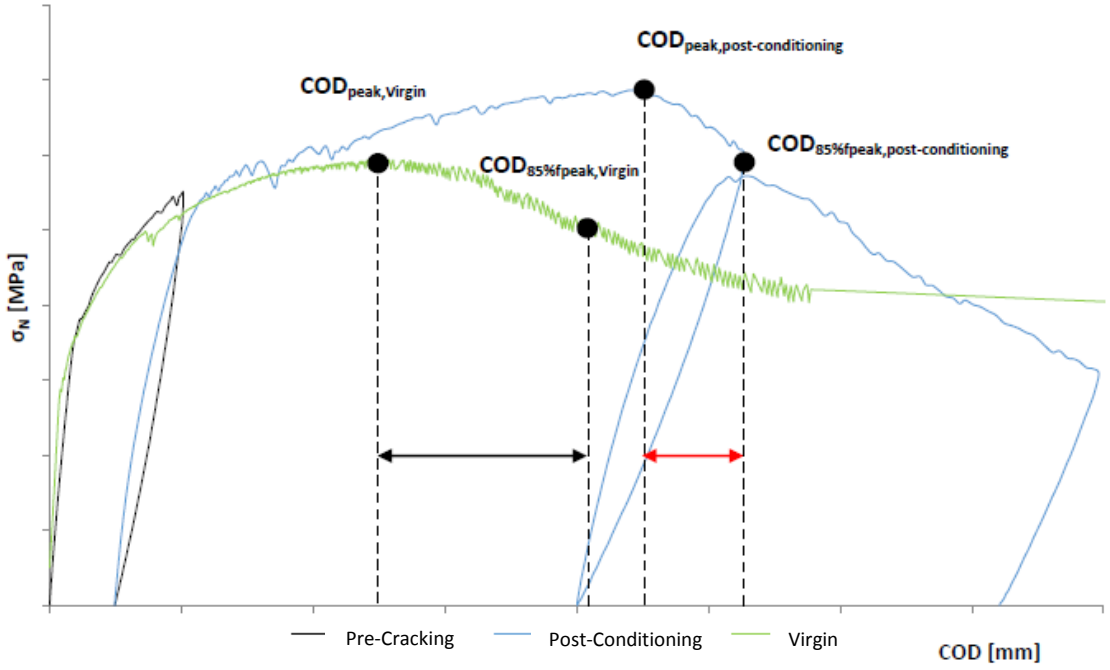

(a)

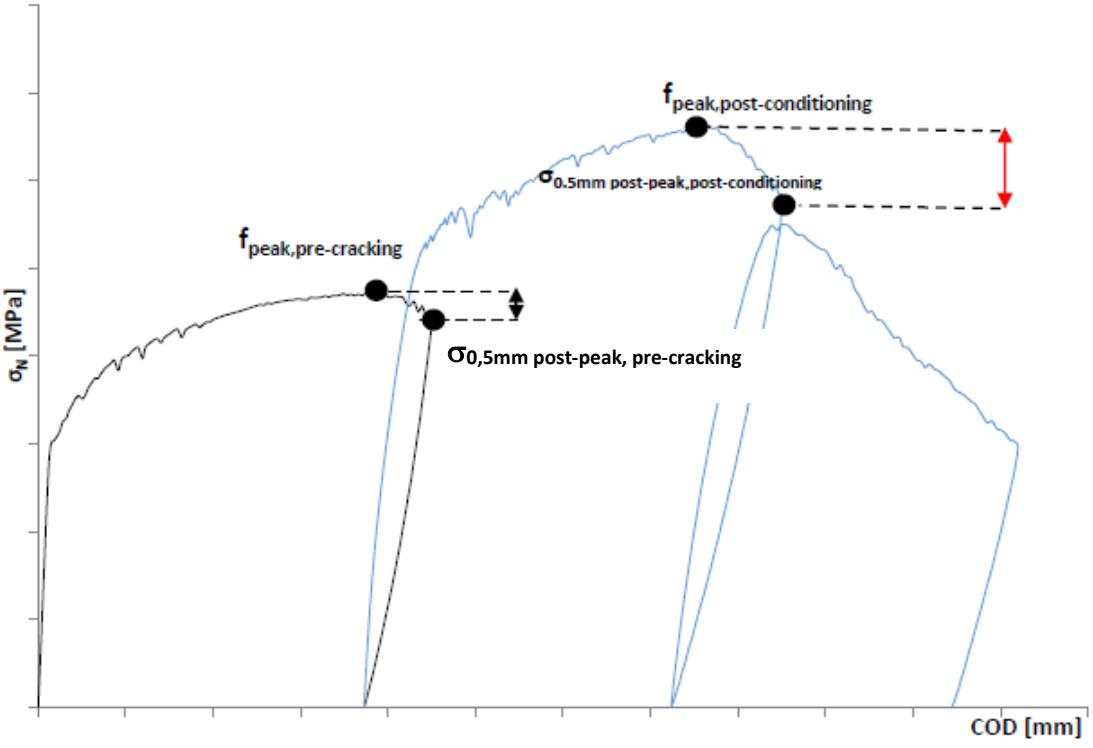

(b)

Figure 18. Notation and definition of the parameters for the Index of Ductility Recovery for deflection hardening specimens pre-cracked in the pre-peak (a) and post-peak regime (b).

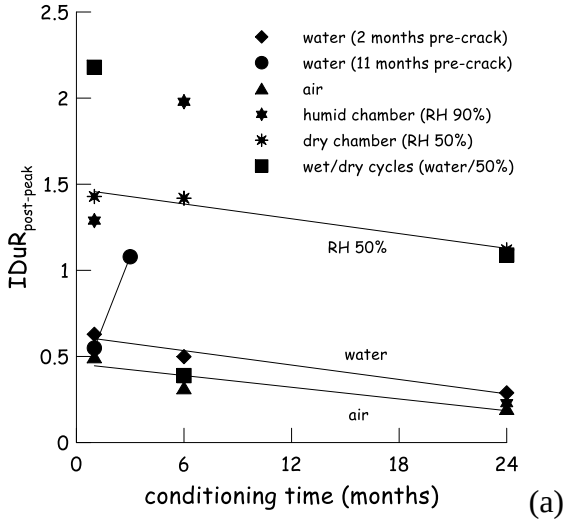

(a)

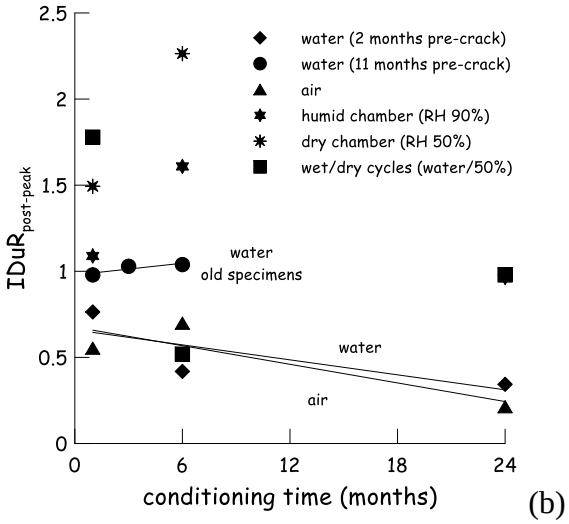

(b)

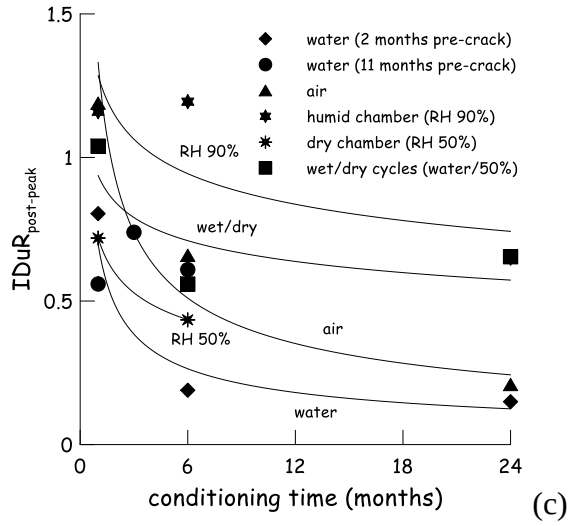

(c)

Figure 19. Index of post-peak Ductility Recovery vs. conditioning time for deflection hardening specimens pre-cracked up to 1 mm (a), 2 mm(b) and 0.5 mm after the peak (c).

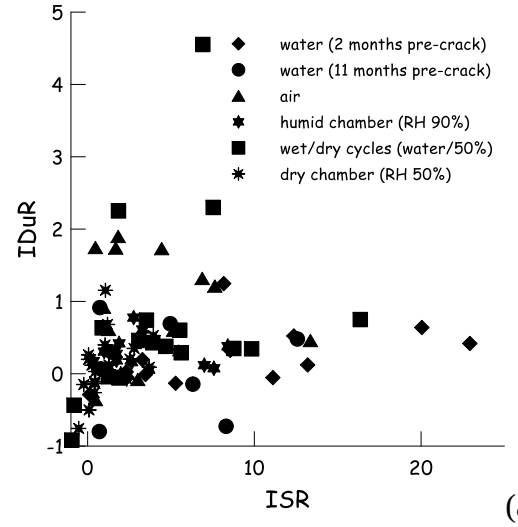

(a)

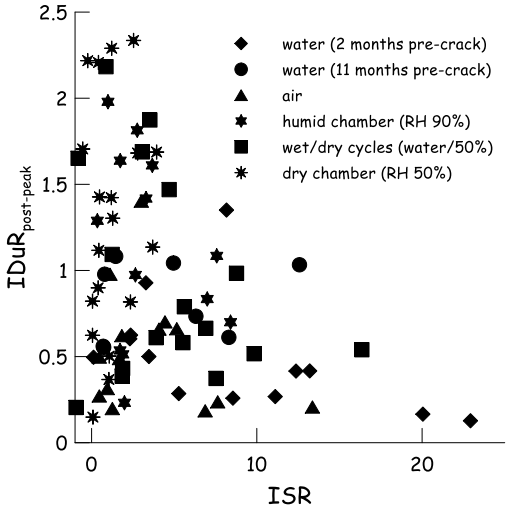

(b)

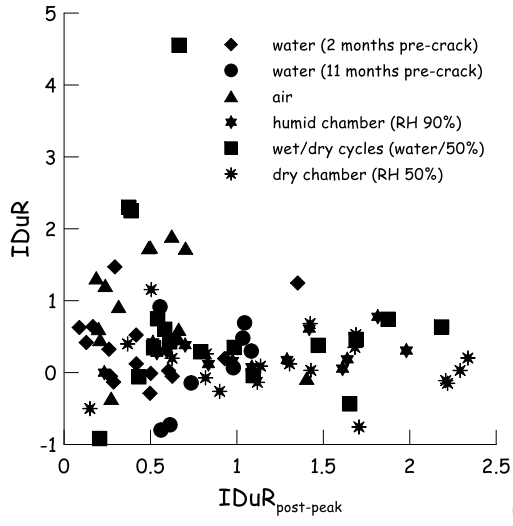

(c)

Figure 20. Correlation between Index of Ductility Recovery (a) and Index of post-peak Ductility Recovery (b) vs. Index of Stress Recovery and between the two indices of Ductility Recovery (c) - for deflection-hardening specimens only.

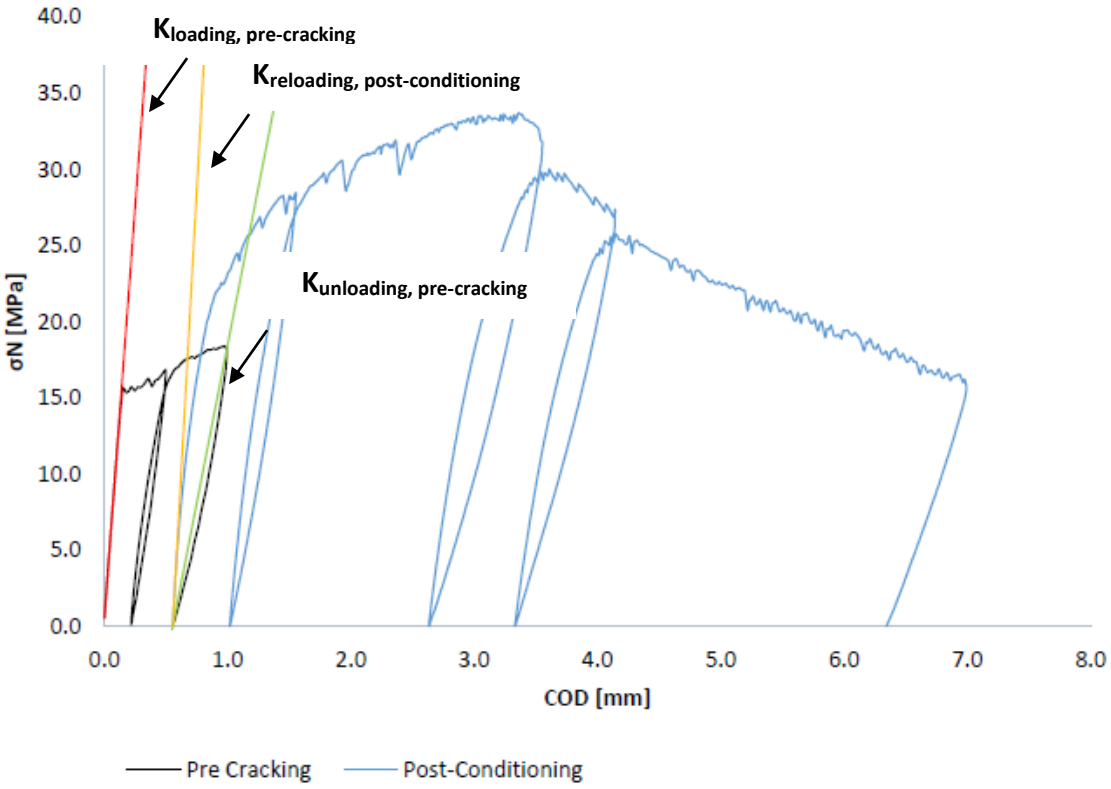

Figure 21: notation for the calculation of Index of Damage Recovery.

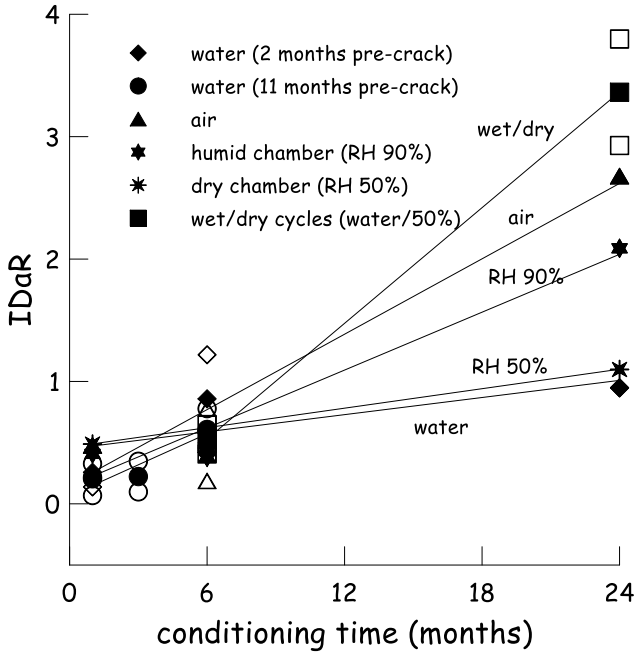

Figure 22. Index of Damage Recovery vs. conditioning time for deflection softening specimens (hollow markers refer to values of single tests, solid markers represent average values of nominally identical tests).

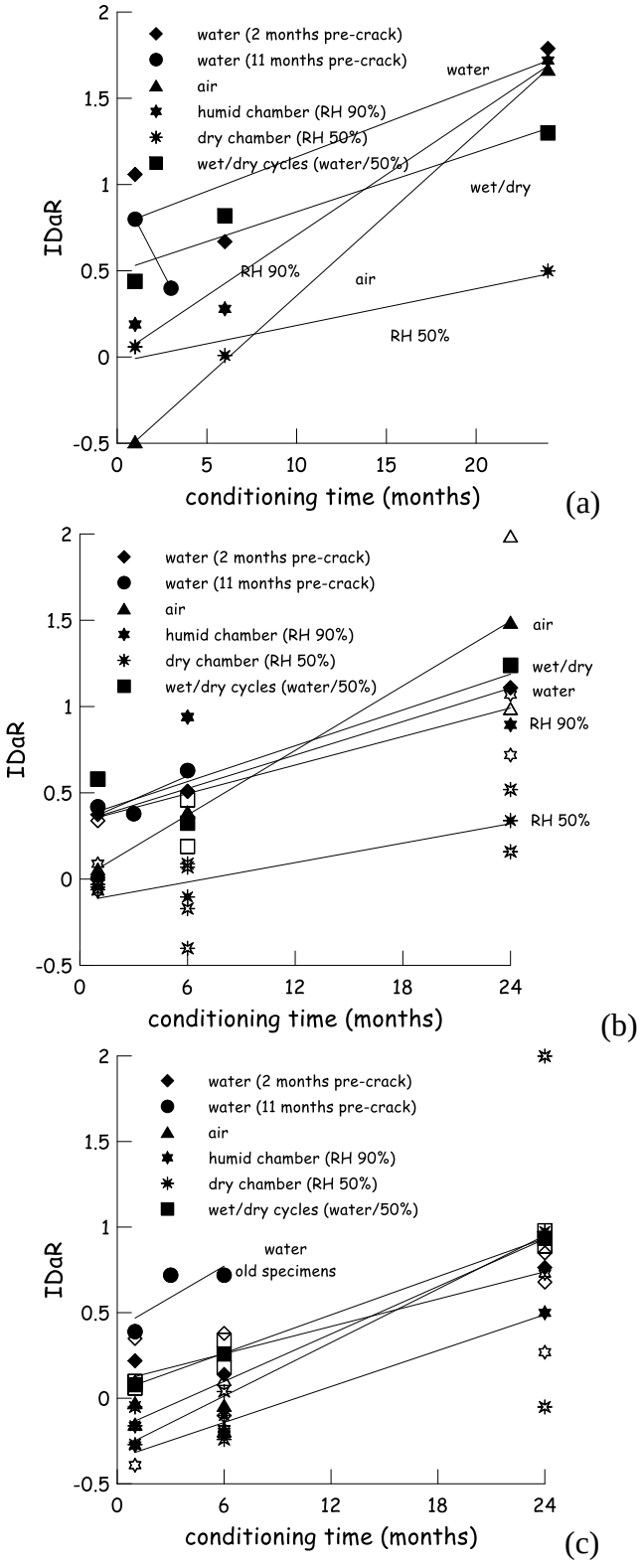

Figure 23. Index of Damage Recovery vs. conditioning time for deflection hardening specimens pre-cracked up to 1 mm (a), 2 mm(b) and 0.5 mm after the peak (c) (hollow markers refer to values of single tests, solid markers represent average values of nominally identical tests).

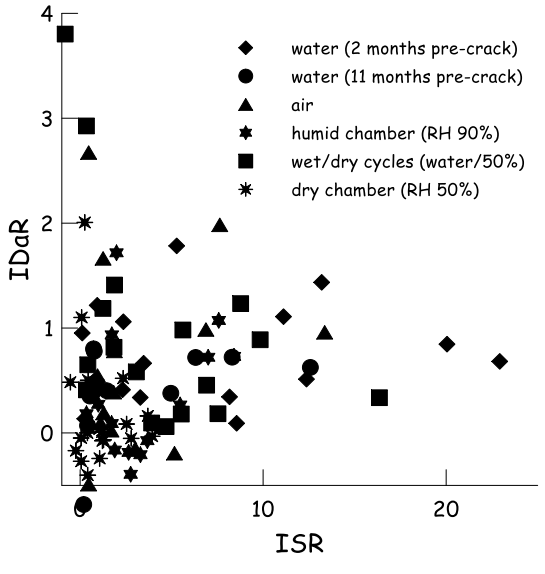

(a)

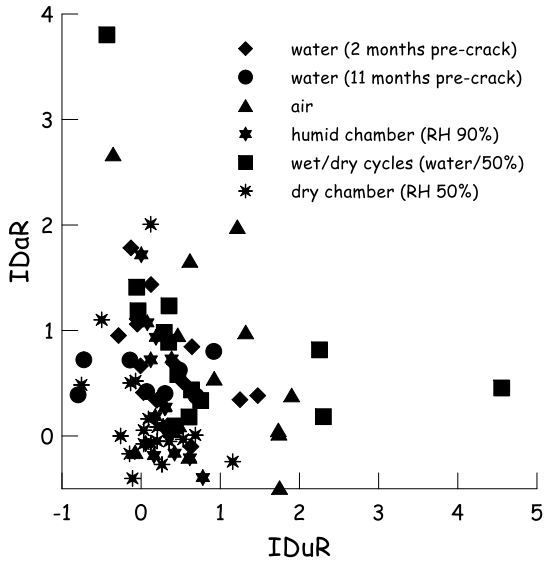

(b)

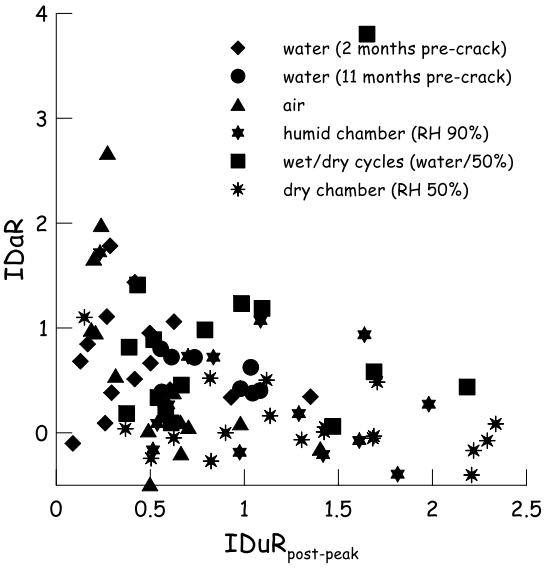

(a)

Figure 24. Correlation between IDaR and ISR (a), IDuR (b) and $IDuR_{post\text{-}peak}$ (c).

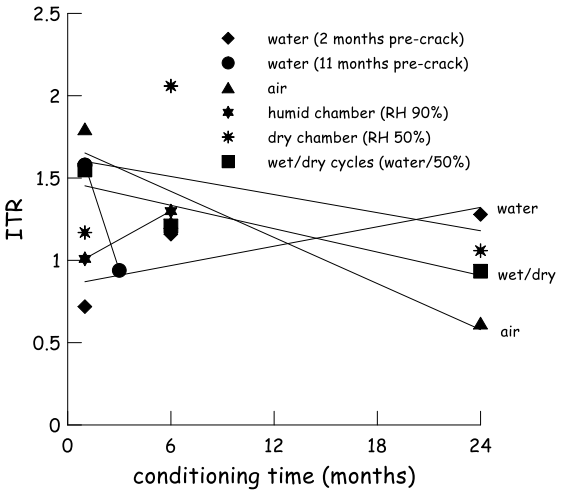

(a)

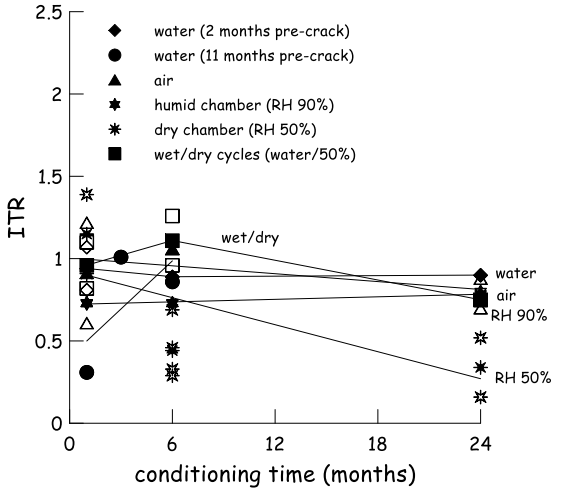

(b)

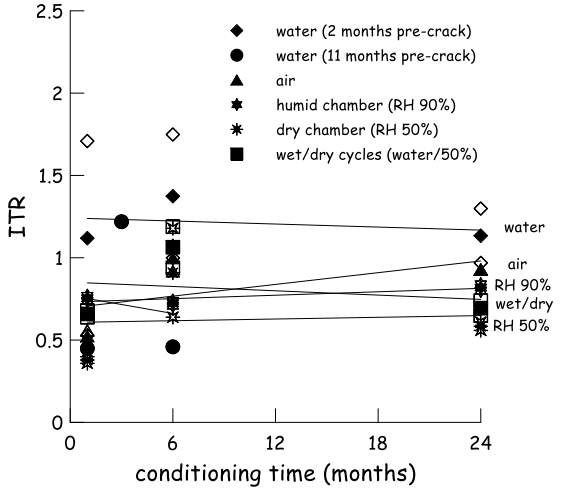

(c)

Figure 25. Index of Toughness Recovery vs. conditioning time for deflection hardening specimens pre-cracked up to 1 mm (a), 2 mm(b) and 0.5 mm after the peak (c) (hollow markers refer to values of single tests, solid markers represent average values of nominally identical tests).

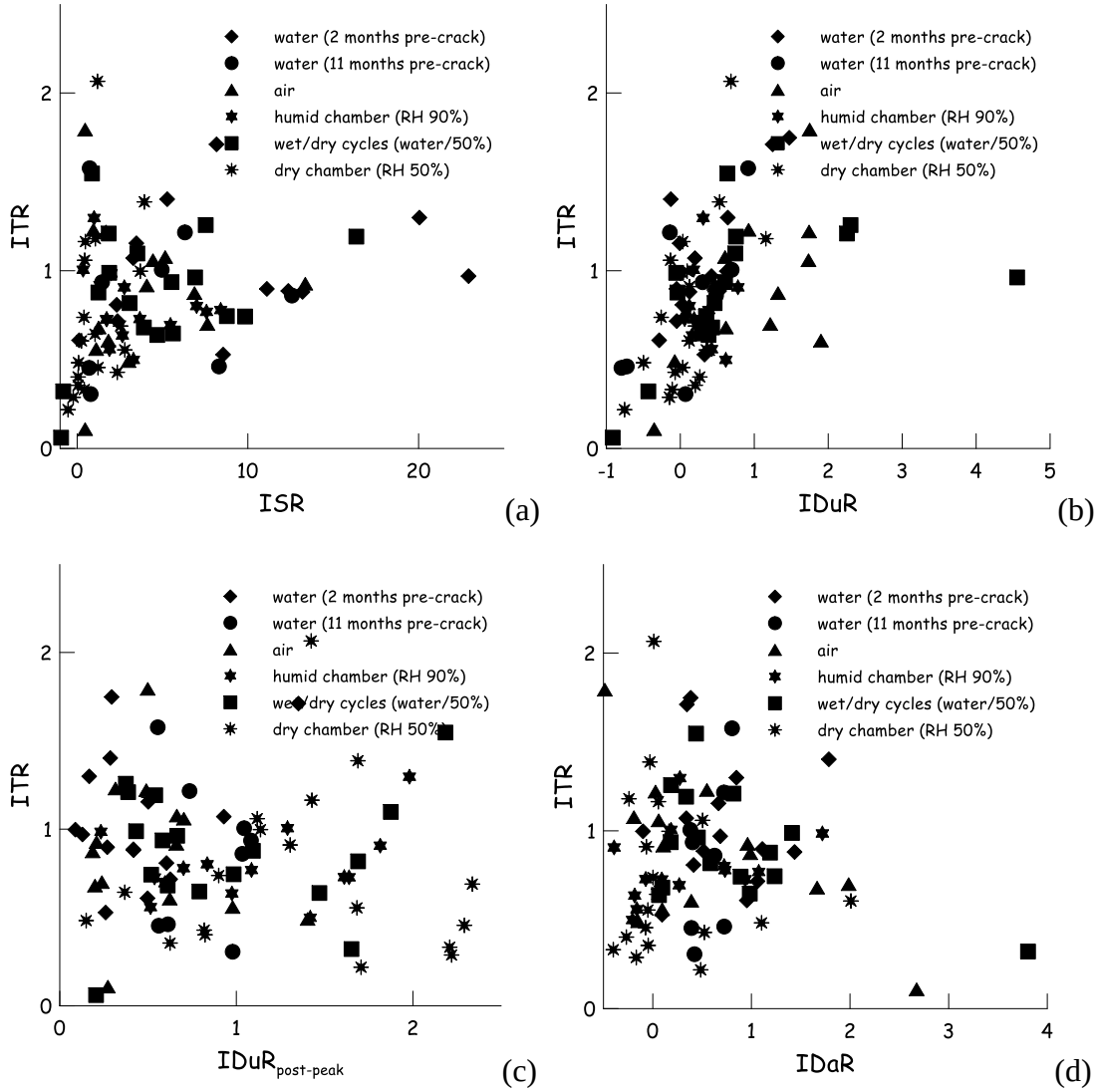

Figure 26. Correlation between Index of Toughness Recovery and Index of Stress Recovery (a); Index of peak (b) and post-peak (c) Ductility recovery and Index of Damage Recovery (d).

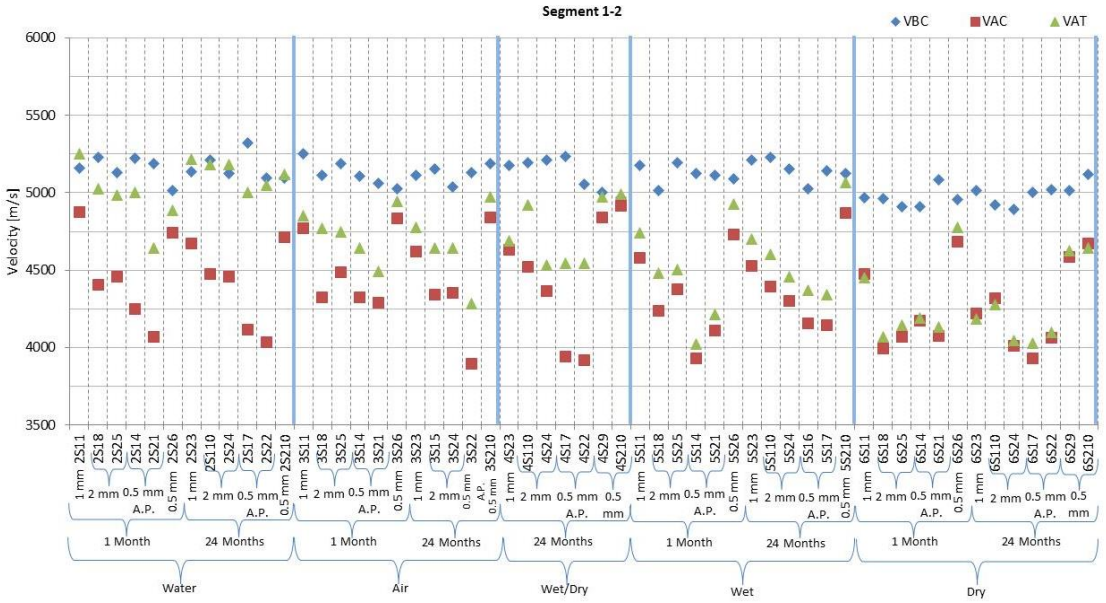

(a)

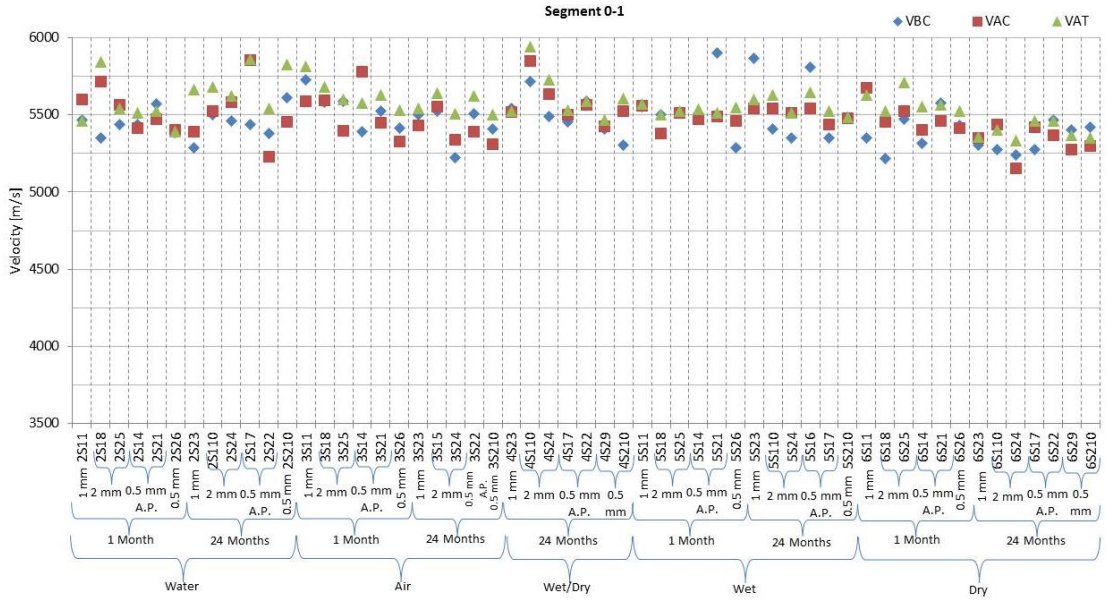

(b)

Figure 27. Ultrasonic Pulse Velocities measured before cracking (VBC in notation), after pre-cracking (VAC) and after conditioning treatments (VAT) in the central cracked (a) and in the left undamaged (b) portions of the specimens.

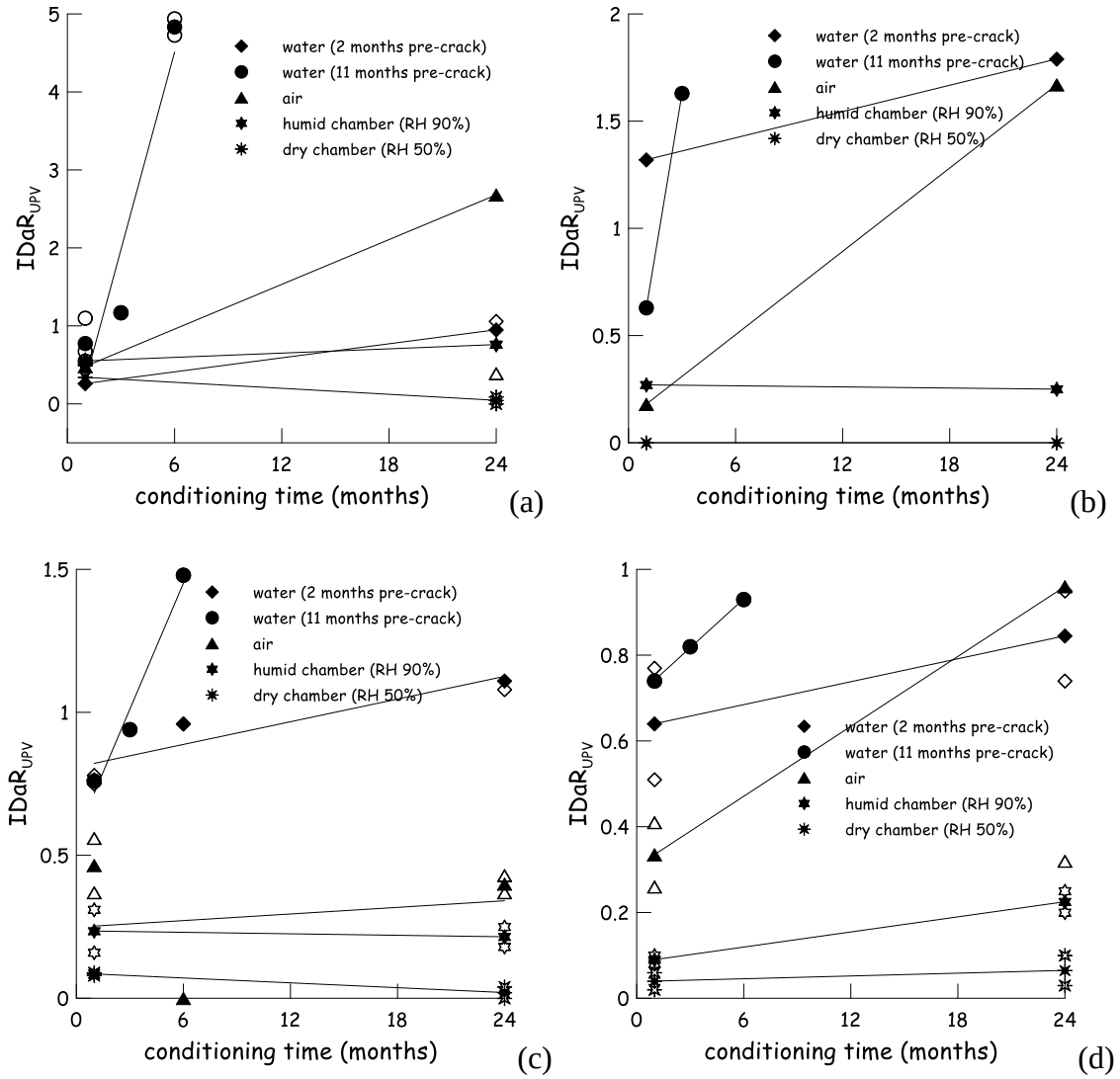

Figure 28. Index of Damage Recovery as per UPV tests vs. conditioning time for deflection softening (a) and deflection hardening specimens pre-cracked up to 1 mm (b), 2 mm (c) and 0.5 mm after the peak (d) (hollow markers refer to values of single tests, solid markers represent average values of nominally identical tests).

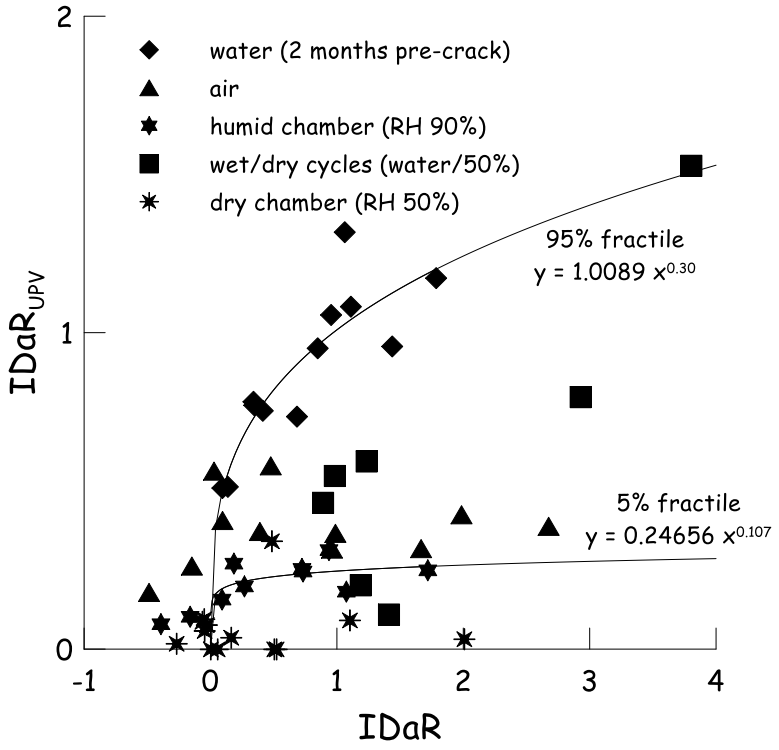

Figure 29: Correlation between Index of Damage Recovery as per UPV tests and Index of Damage recovery as per 4pb tests (b).

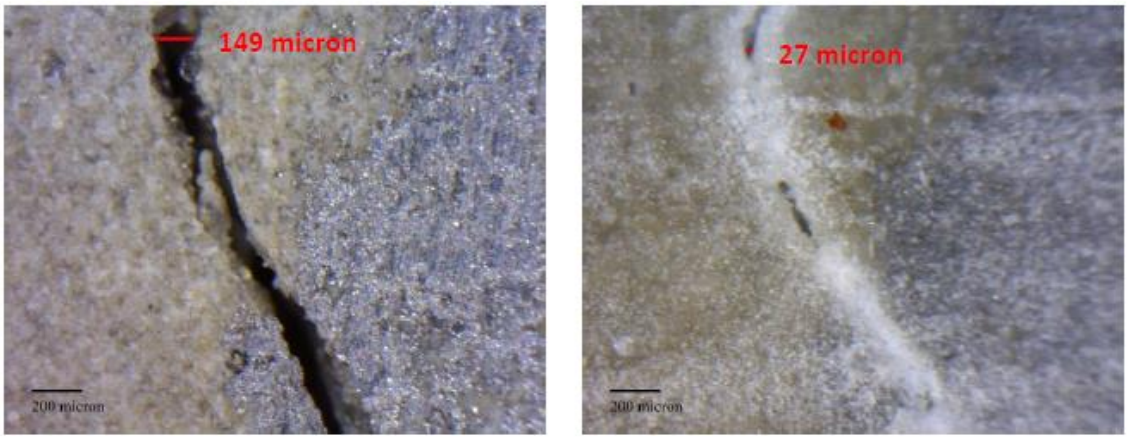

(a)

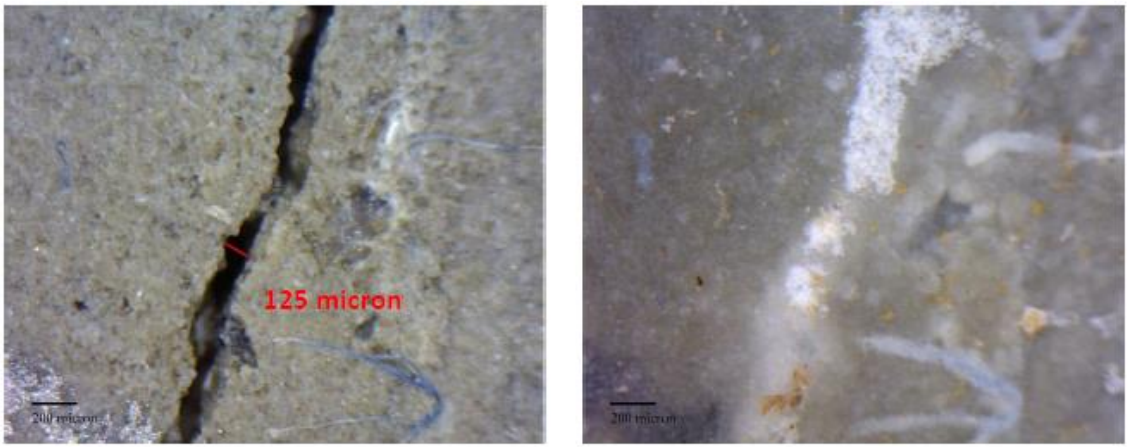

(b)

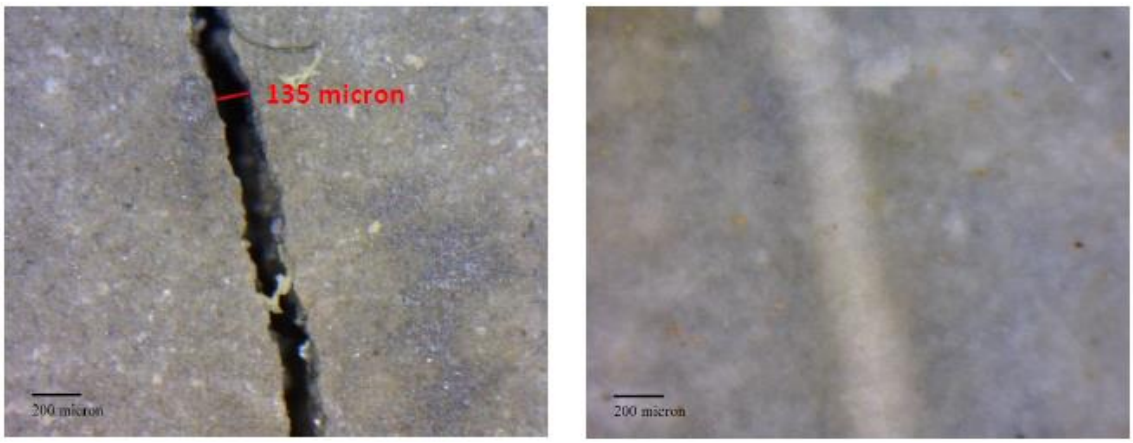

(c)

Figure 30. Examples of healed cracks of specimens pre-cracked at 2 months age and immersed in water for 1 (a), 6 (b) and 24 (c) months.

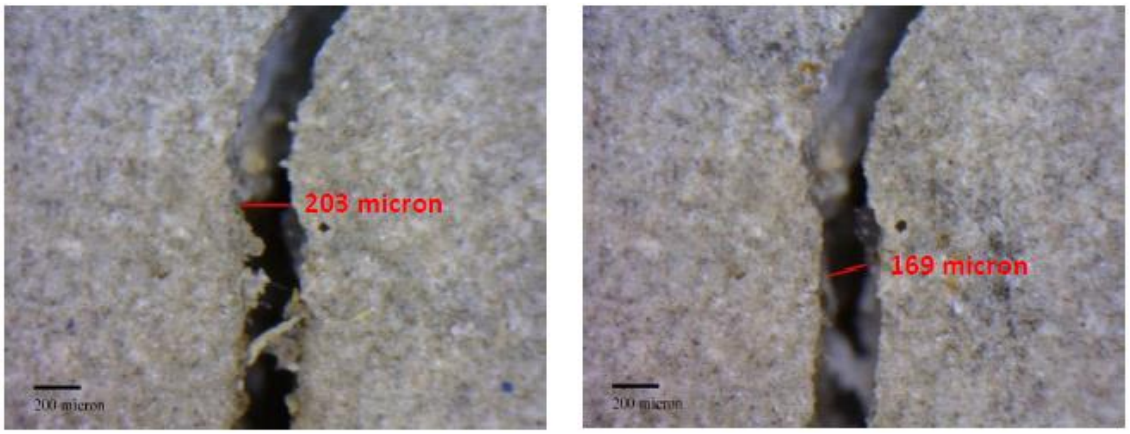

(a)

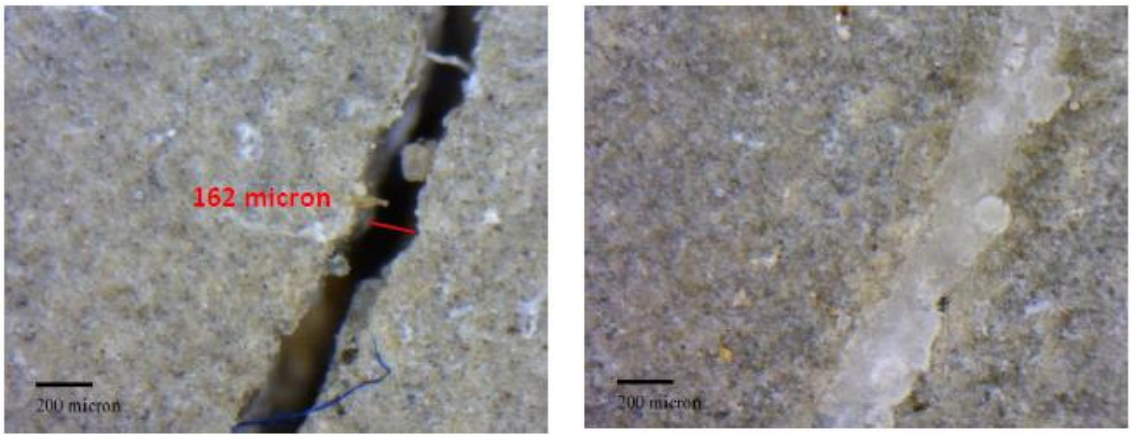

(b)

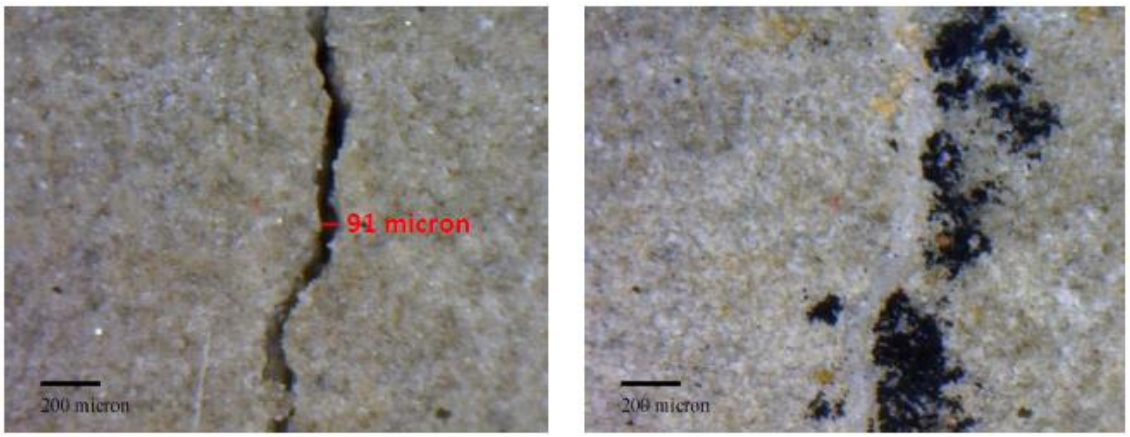

(c)

Figure 31. Examples of healed cracks of specimens pre-cracked at 9/11 months age and immersed in water for 1 (a), 3 (b) and 6 (c) months.

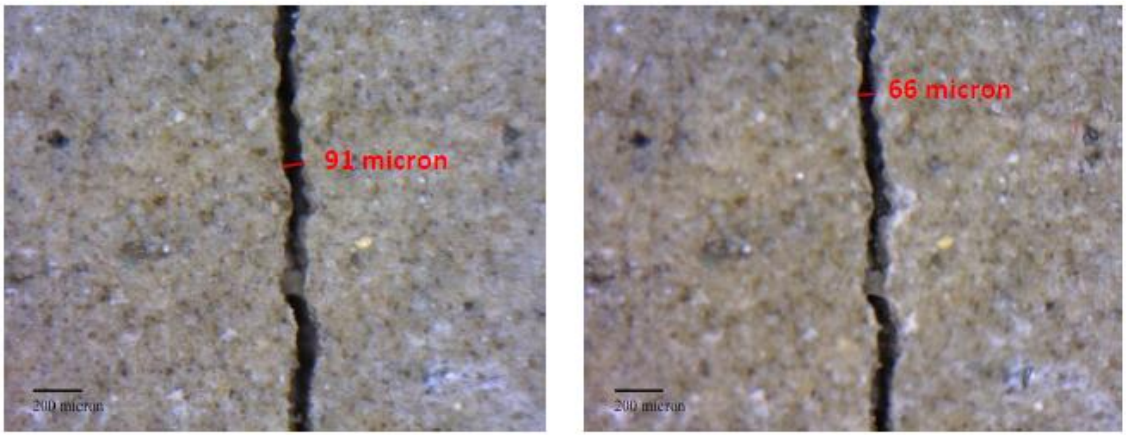

(a)

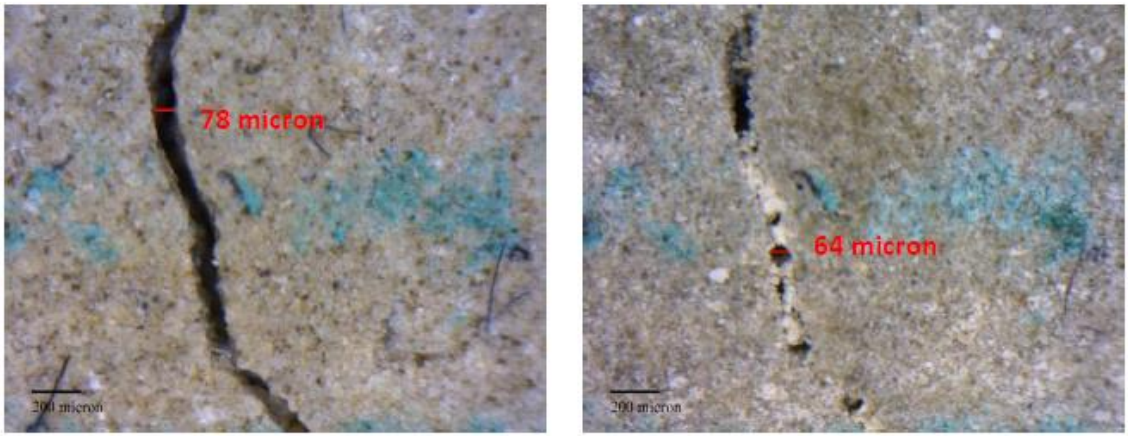

(b)

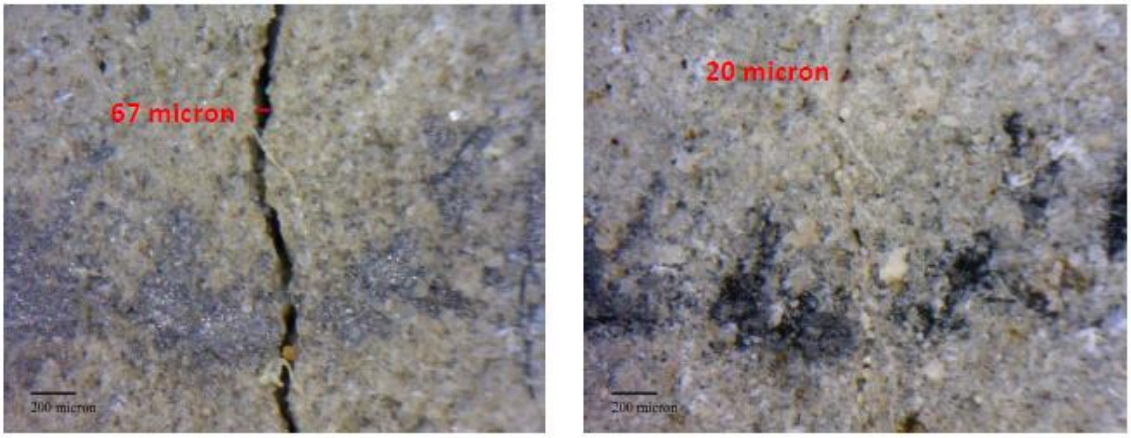

(c)

Figure 32. Examples of healed cracks of specimens pre-cracked at 2 months age and exposed to open air for 1 (a), 6 (b) and 24 (c) months.

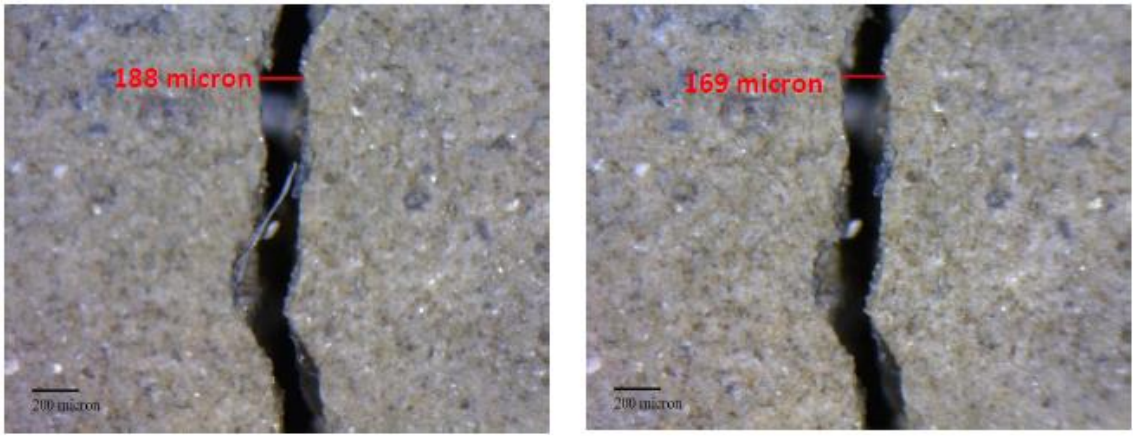

(a)

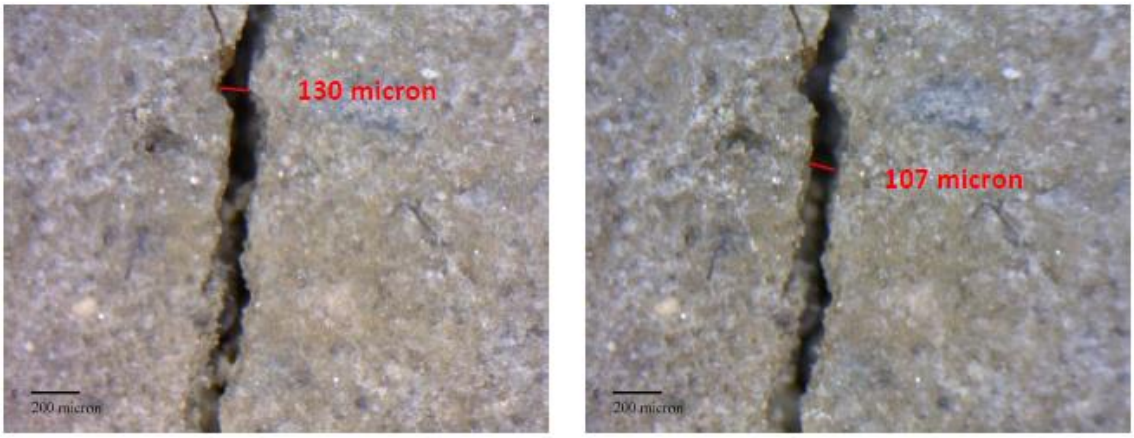

(b)

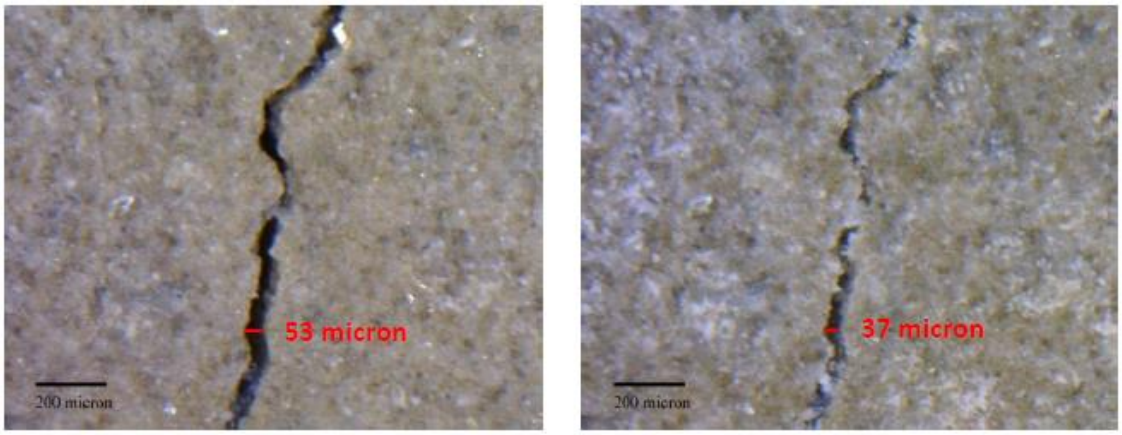

(c)

Figure 33. Examples of healed cracks of specimens pre-cracked at 2 months age and exposed to RH 90% for 1 (a), 6 (b) and 24 (c) months.

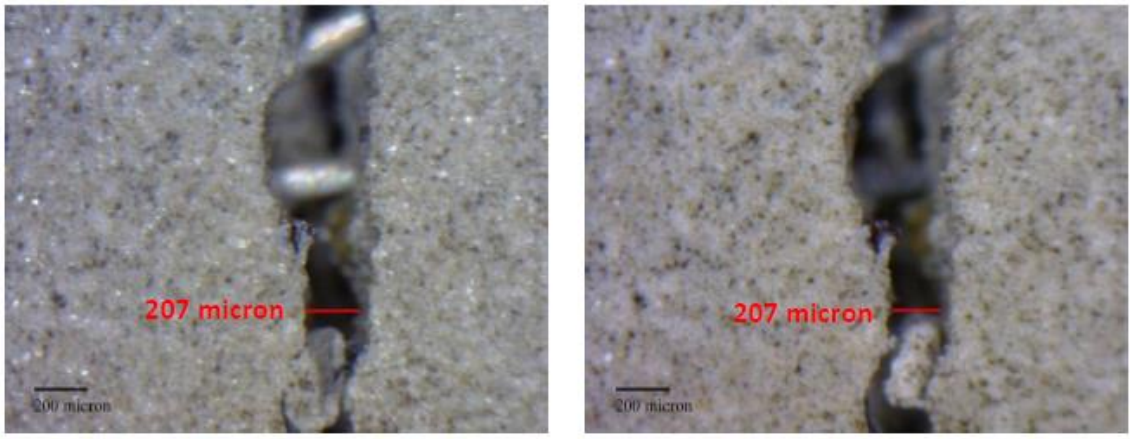

(a)

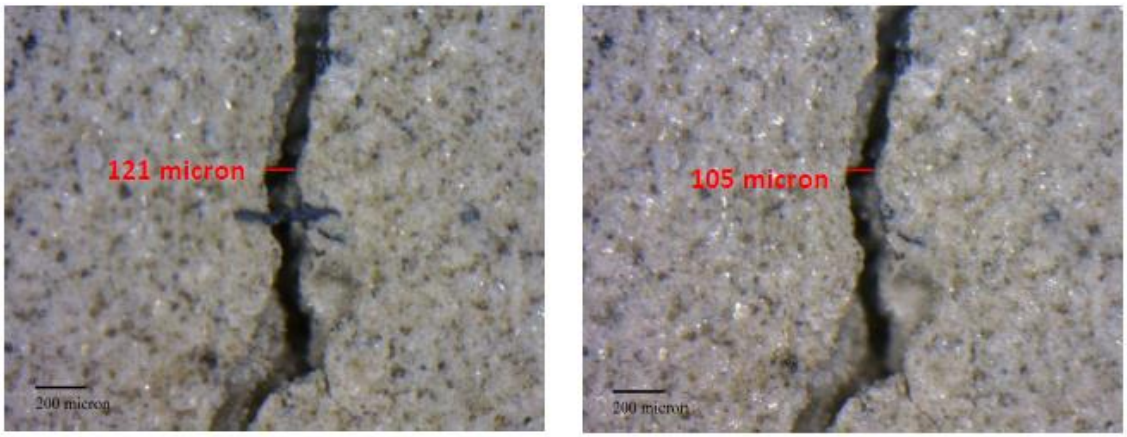

(b)

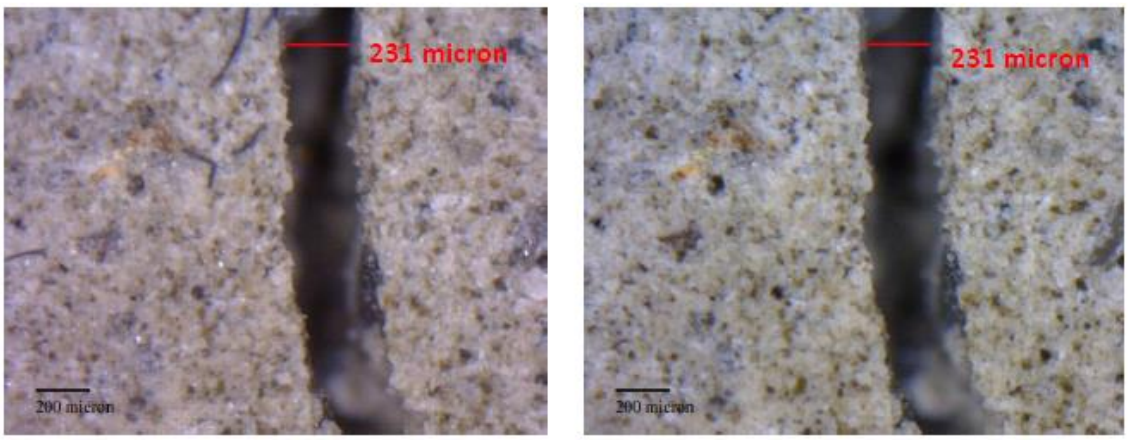

(c)

Figure 34. Examples of healed cracks of specimens pre-cracked at 2 months age and exposed to RH 50% for 1 (a), 6 (b) and 24 (c) months.

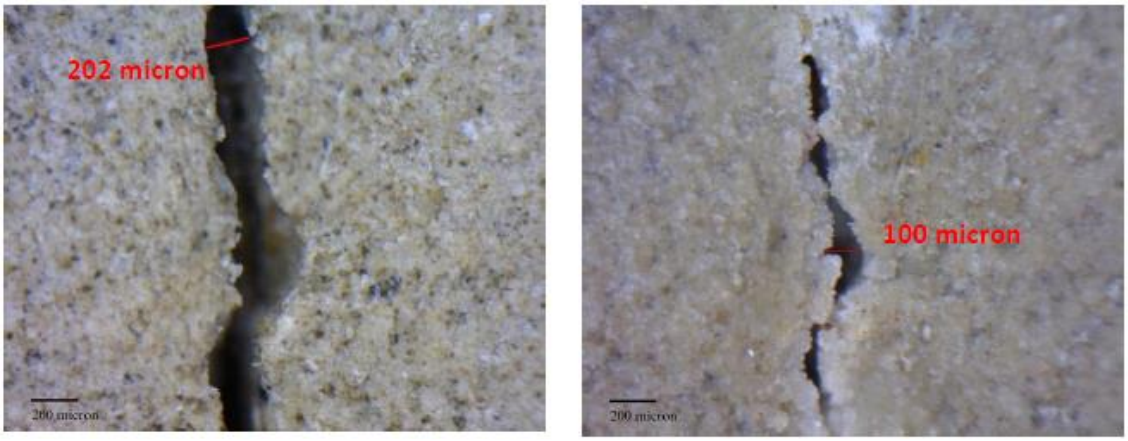

(a)

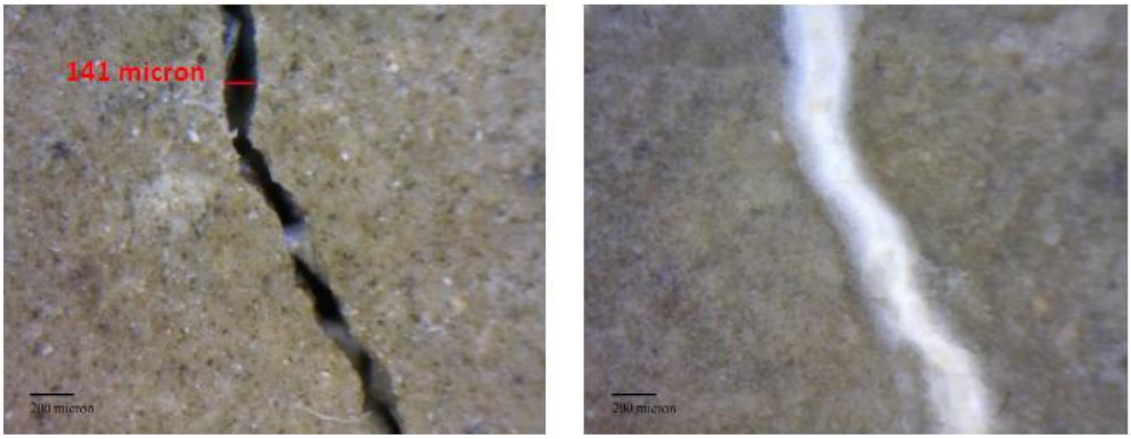

(b)

Figure 35. Examples of healed cracks of specimens pre-cracked at 2 months age and exposed wet and dry cycles for 1 (a) and 24 (b) months.

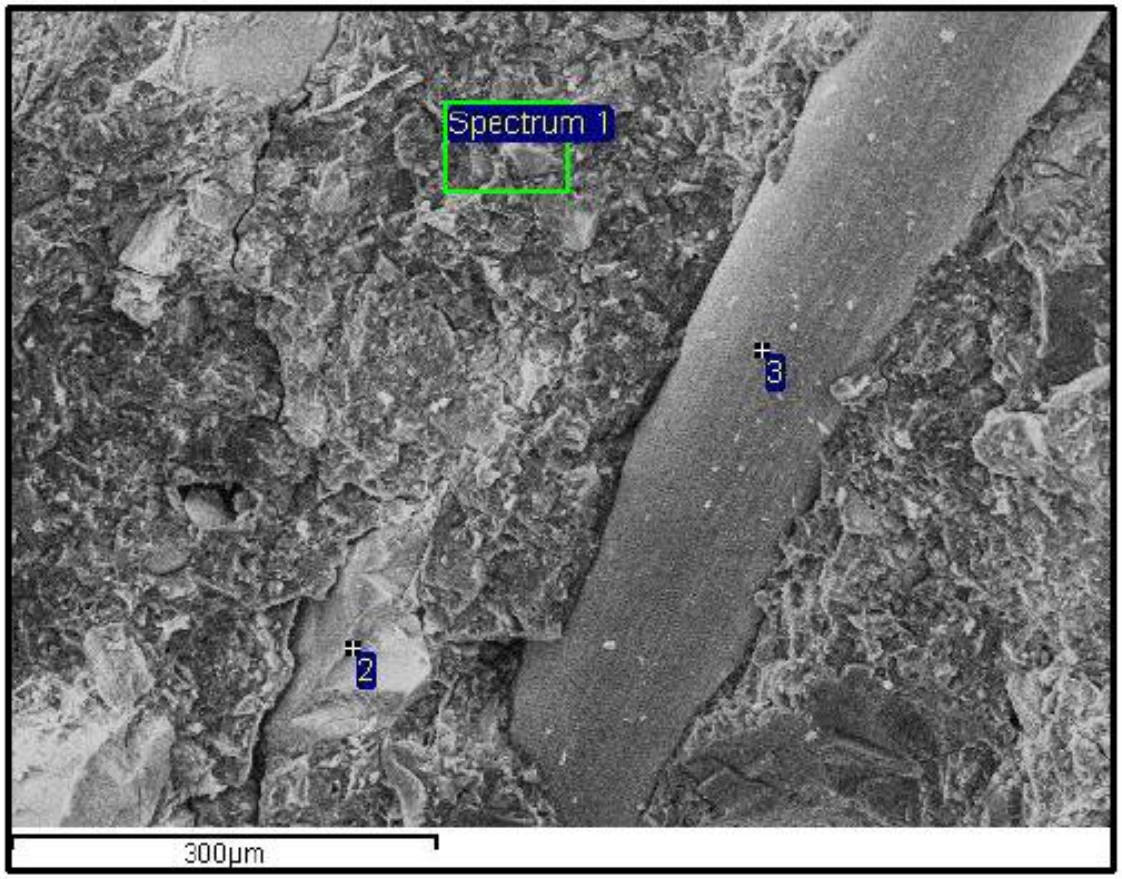
Spectrum 1
2
3
300µm

(a)

60

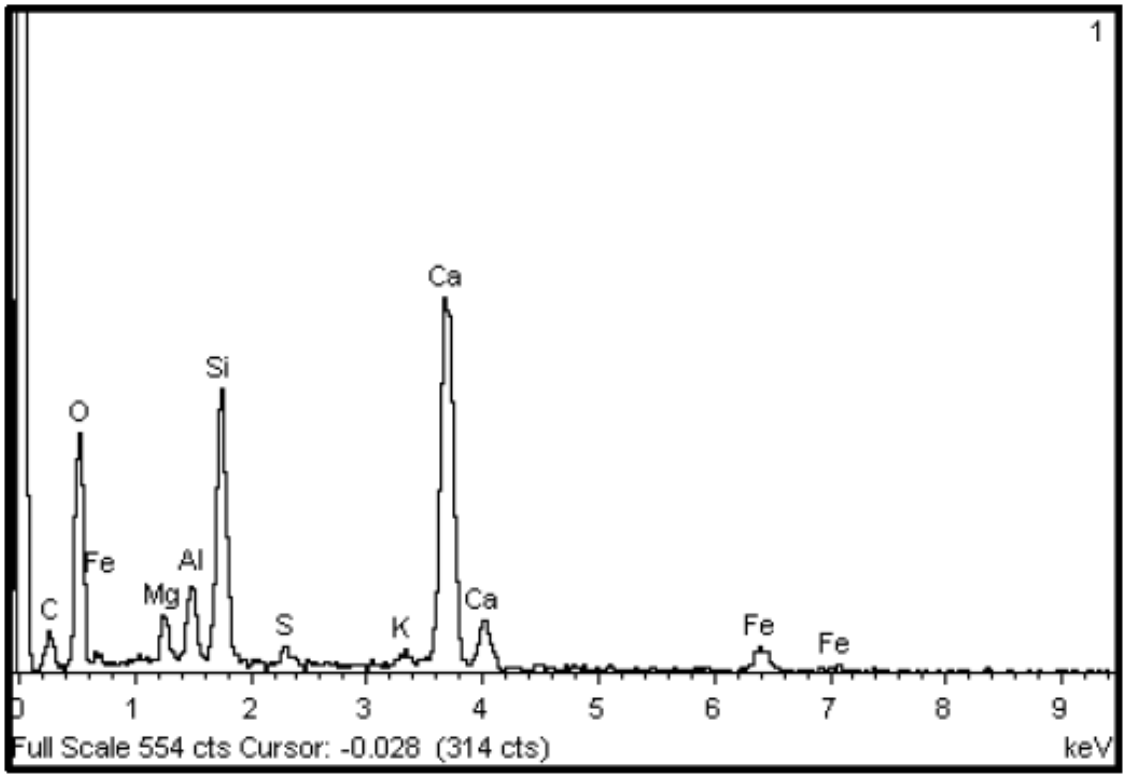
1
Ca
Si
O
Fe
Al
Mg
C
S
K
Ca
Fe
Fe
0
1
2
3
4
5
6
7
8
9
Full Scale 554 cts Cursor: -0.028 (314 cts)
keV

(b)

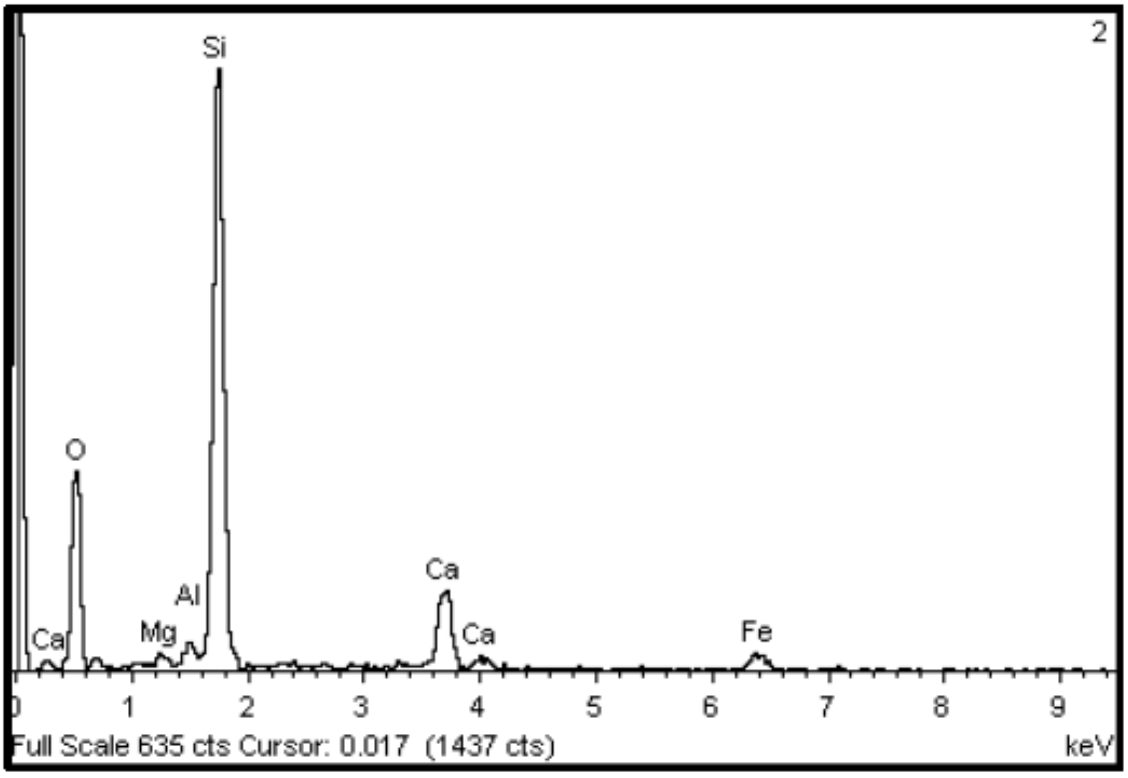

(c)

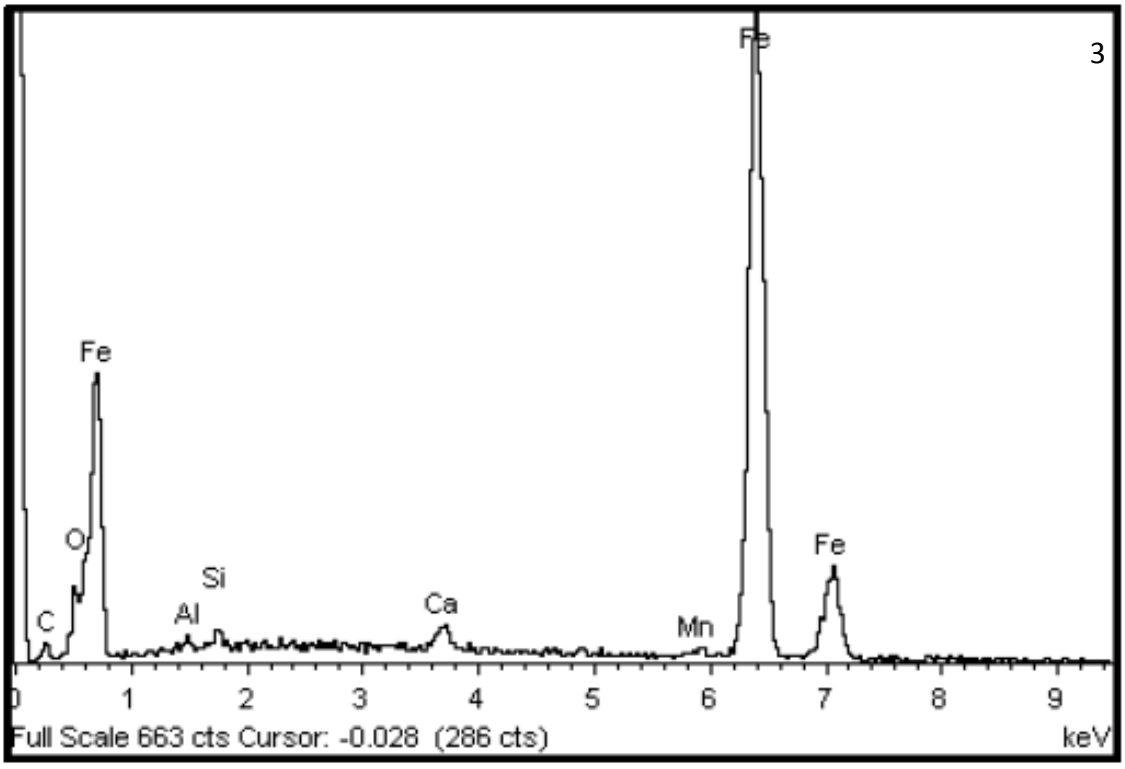

(d)

Figure 36. Microscopy image of a "healed" fracture surface (a) and SEM analysis of cement paste (b), sand grain (c) and a fibre (d).